



Schweizer Kompetenzzentrum
für Tiefengeothermie zur
Strom- und Wärmeproduktion
ein Unternehmen von



Technical Note:

Assessment of the seismic risk induced by the geothermal project of Haute- Sorne

Authors:

Dr. Falko Bethmann

Olivier Zingg

Version 9. Mar. 2015

Updated version from Nov. 25th 2014 report, incorporates answers to questions of BAFU & Canton,
includes Lorca, 2011 case and calculation of injuries as well as individual risk

Summary

Based on the logic tree method described in Mignan et al., 2015 we determine seismic risk for a deep geothermal project in the community of Haute-Sorne, Jura, Switzerland. Branches of the logic tree and parameter settings were selected after discussion with experts of the Swiss Seismological Service. The results are compared with empirical data of induced or natural events in Switzerland or surrounding countries.

We present a best estimate of insured value loss for a magnitude $M_w=4$ event and a magnitude $M_w=5$ event leading to a loss of 0.62 Mio. and 21.7 Mio. CHF, respectively. To obtain a measure of risk, hazard estimates are combined with 3 different magnitude frequency distributions. Uncertainties at the hazard and risk level are considered in a systematic way.

To illustrate risk, we present exceedance probabilities for intensities as well as financial losses and casualties. We compare results to the Swiss ordinance on the prevention of major accidents (Störfallverordnung, StFV or Ordonnance sur la protection contre les accidents majeurs, OPAM). Based on OPAM, the presented risks are considered as acceptable.

Table of contents

Summary.....	2
1 Introduction	4
2 Method	4
2.1 Verification:	5
3 Damage scenarios M=4 and M=5 Recommendation 1 of the Swiss Seismological Service.....	7
3.1 Input	7
3.2 Results	7
3.3 Sensitivities and uncertainties.....	8
3.4 Comparison to three earthquake scenarios in the surroundings or within Switzerland	10
3.5 Discussion & Conclusion.....	11
4 Probabilistic Risk (recommendation 2 of the Swiss Seismological Service).....	11
4.1 Input	12
4.2 Results and sensitivity analysis to key parameters	13
4.3 Discussion.....	19
5 Risk in the framework of OPAM.....	19
5.1 Casualties	20
5.2 Financial risk judged by OPAM	20
6 Individual risk.....	21
6.1 Method.....	21
6.2 Input	22
6.3 Results	23
6.4 Discussion.....	24
7 Conclusion.....	25
8 References	27
A. Empirical data	29
A.1. List of earthquakes and sources.....	29
A.2. Corrections and conversions.....	30
B. EMS 98 Intensity scale	33
C. Explanation of exceedance probability and rate of occurrence	34
D. Injuries	36
E. Additional plots including all branches	38
F. Geothermics paper, Mignan et al., 2015	45

1 Introduction

In the framework of an environmental impact assessment study for a geothermal pilot project in the community of Haute-Sorne, Geo-Energie Suisse AG has presented a deterministic and a probabilistic seismic hazard study.

As independent assessor the Swiss Seismological Service (SED) has reviewed both studies and proposed two recommendations that lead to a better representation of seismic risk. Geo-Energie Suisse AG has incorporated the suggestions of the SED and presents the results in the following.

By a later request the Canton of Jura also demanded a comparison of risk (including casualties) with the Swiss ordinance on the prevention of major accidents (OPAM). Therefore, an extra chapter discussing risk in the framework of OPAM is also added.

2 Method

Aim of the study is to present a best estimate of seismic risk and losses caused by earthquakes. At present, information about the seismic response of the underground is yet unknown. Therefore, a broad variation of 'physical realities' is considered including also inherent uncertainty. To treat uncertainties in a systematic way, we follow a logic tree approach (Mignan et al., 2015). After discussions with experts of the Swiss Seismological Service (SED), the method is tailored to what is believed the best setup for induced seismicity in the community of Haute-Sorne.

The method can be separated into two parts: First, a deterministic part (Figure 1, highlighted in red colors), which covers a broad range of possible responses of the underground, which themselves are combined with three different cost functions (denoted as model- or epistemic uncertainty) - and second, a probabilistic part (Figure 1, highlighted in blue colors), that couples the deterministic damage scenarios with three magnitude frequency distributions, including assumptions about the randomness of nature (aleatory variability).

The logic tree consists of 72 branches (3x8x1x3):

- 3 maximum magnitude models derived from a deterministic and a probabilistic study
- 8 (2x2x2) ground motion prediction models that include 2 attenuation parameters (Q), 2 stress drops ($\Delta\sigma$)- and 2 site specific attenuation parameters (κ).
- 1 ground motion intensity conversion equation
- 3 cost functions

The best estimate of (deterministic) losses is considered to be the median out of 8 ground motion prediction equations multiplied by 3 cost functions (red part in Figure 1)

The best estimate of exceeding probabilities for losses is considered to be the median of all 72 branches.

VERTRAULICH

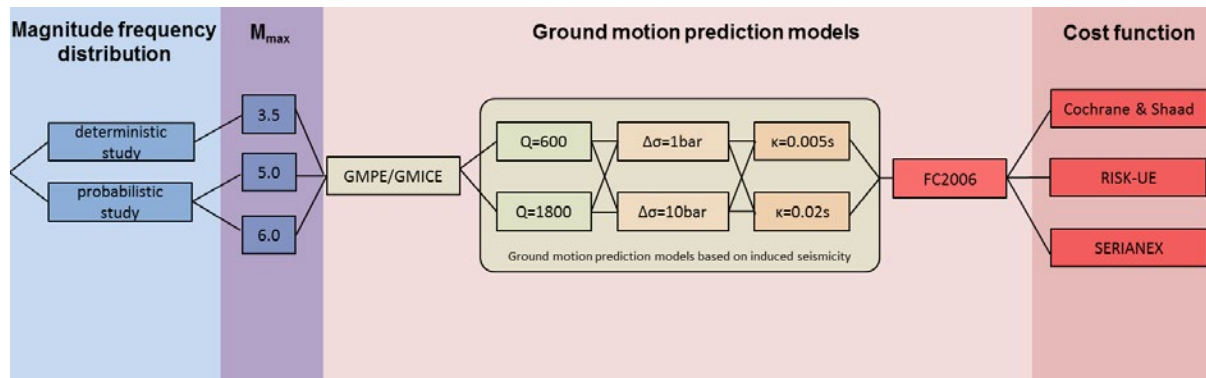


Figure 1: Logic tree to calculate the risk of induced seismicity in the community of Haute-Sorne. All branches are equally weighted. Input are results of the deterministic and probabilistic risk studies submitted in the framework of the environmental hazard assessment. Epistemic uncertainty is covered by a broad variation of ground motion prediction models (GMPEs) and cost functions (red background). GMPEs express ground motion in units of peak ground velocity (pgv). Conversion to intensity, the input to cost functions, is done by a ground motion intensity conversion equation (GMICE). GMPEs are based on Douglas et al., 2013, the GMICE FC2006 refers to Facciolo & Cauzzi, 2006. Cost functions are taken from Cochrane & Schaadt, 1992, Risk UE functions refer to Mouroux & Brun, 2006 and the SERIANEX function refers to the Basel risk study of Baisch, 2006.

2.1 Verification:

The selection of branches is compared to empirical data of induced seismicity in Europe (see Appendix A). The choice of 8 ground motion prediction models (GMPEs) coupled with 3 cost functions captures all data points within their intrinsic uncertainty (Figure 2). On the upper end only one data point is situated above the one standard deviation (1σ) bound, which refers to the Basel geothermal project. In this case it is known, that many damages were compensated out of good will and therefore insured value loss (IVL) is considered to be excessive (Genoni, 2013 & Mignan et al., 2015). 4 data points are below the 1σ bound, all referring to events before 1992. Two of them refer to mine blasts & collapses in the former German Democratic Republic, where actual damage might be higher than reported due to political reasons. In total 7 data points fall above the median, 14 below.

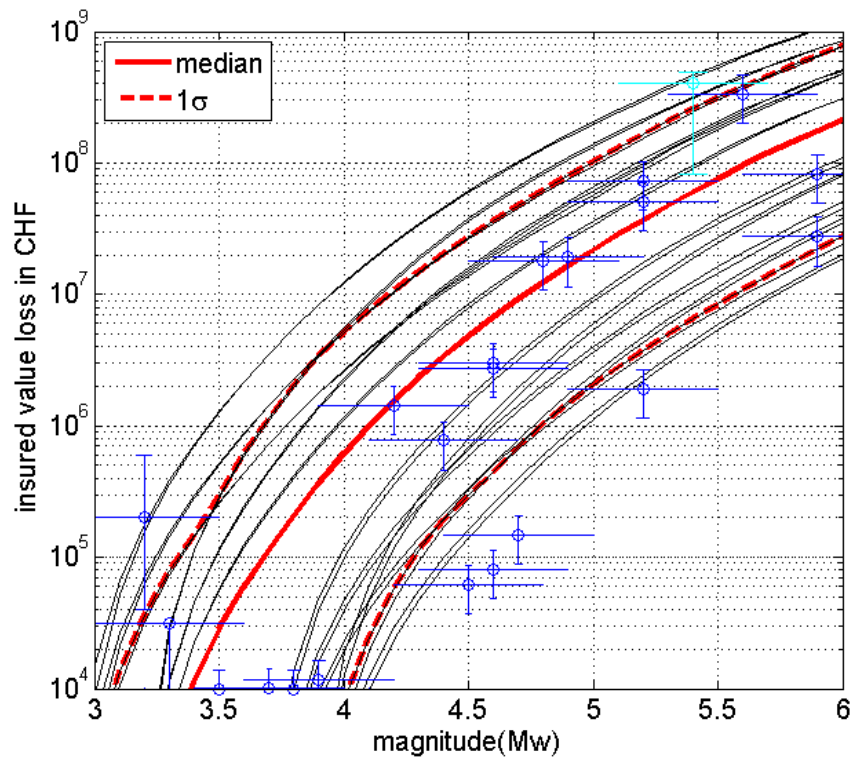


Figure 2: Empirical validation of loss curves. Shown in black are predicted losses based on 8 ground motion prediction equations coupled with 3 cost functions (red part of the logic tree in Figure 1). Shown in blue is magnitude-damage data from the literature, corrected by population density and hypocentral depth. Plotted in cyan color is the highest loss event, the earthquake of Lorca in 2011. The median is used to highlight the best estimate; ± 1 standard deviation shows 68% of the total hazard distribution.

3 Damage scenarios M=4 and M=5

Recommendation 1 of the Swiss Seismological Service

Recommendation 1:

We suggest that the operators compute risk scenarios for a magnitude M4.0 and M5.0 event to illustrate the consequences of such very unlikely but potentially damaging earthquakes

3.1 Input

Damage assessment for each branch (Figure 1, red part) is identical to the scientific report E4¹ of the main investigation. The method is also described in Baisch, 2009 and Mignan, 2015. Inputs to cost functions are intensity estimates derived by the 8 different ground motions for every village within 20 km around the heat exchanger. Surface amplification effects are corrected by +0.47 intensity units.

Building stock information of all villages is taken from the website of the Swiss Federal Office for Statistics, average building value is adopted from SERIANEX for Basel Land (avg. bldg. value is 1.449 Mio CHF). Vulnerability index values V0 are defined for each building class. Less probable ranges of V-/V+ and V--/V++ are not considered.

3.2 Results

Damages related to magnitude Mw=4 and Mw=5 events are summarized in Table 1 & Figure 3. The best estimate is considered to be the median of all physical models used for the calculation of damage. A magnitude Mw=4 event leads to an insured value loss of 0.62 Mio. CHF, an event of magnitude Mw=5 leads to a damage of 21.7 Mio CHF. An estimate of damages covering the range of $3 \leq Mw \leq 5$ is shown in Figure 3. Results are validated with empirical data (Chapter 2.1 Validation).

¹ Q-con GmbH: Bewertung des seismischen Risikos durch ein EGS Projekt in der Gemeinde Haute-Sorne; Hauptuntersuchung

Magnitude	Mw=4	Mw=5
median	0.62 Mio CHF	21.7 Mio. CHF
+1 sigma	5.17 Mio. CHF	102.3 Mio. CHF
-1 sigma	< 10'000 CHF	2.17 Mio. CHF

Table 1: Insured value loss estimates for earthquakes of magnitude Mw=4 and Mw=5.

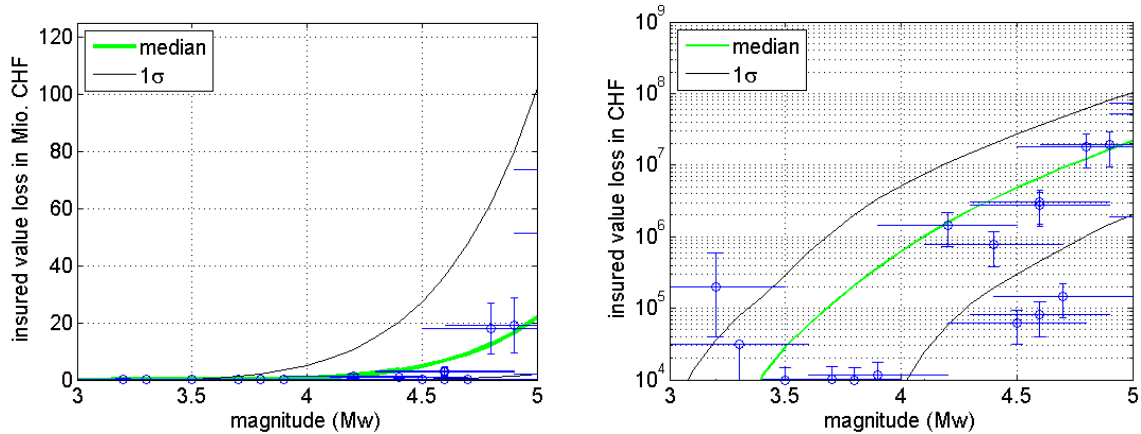


Figure 3: Calculated insured value loss presented in linear and log scale. The best estimate of models is shown in green. Black curves show the epistemic uncertainty of physical models expressed as 1 standard deviation.

3.3 Sensitivities and uncertainties

Regarding uncertainty two terms are used in hazard analysis: epistemic uncertainty and aleatoric variability. Epistemic uncertainty describes the scientific uncertainty within a model, aleatoric variability characterizes the natural randomness in a process. In the following the sensitivity of results with regard to the choice of parameters is described.

Epistemic uncertainty

In the following the sensitivity of calculated losses to the choice of parameters is discussed. To visualize the parameter choice of stress drop, crustal and site specific attenuation as well as cost functions, the respective branches of the tree model are plotted in different colors (Figure 4).

VERTRAULICH

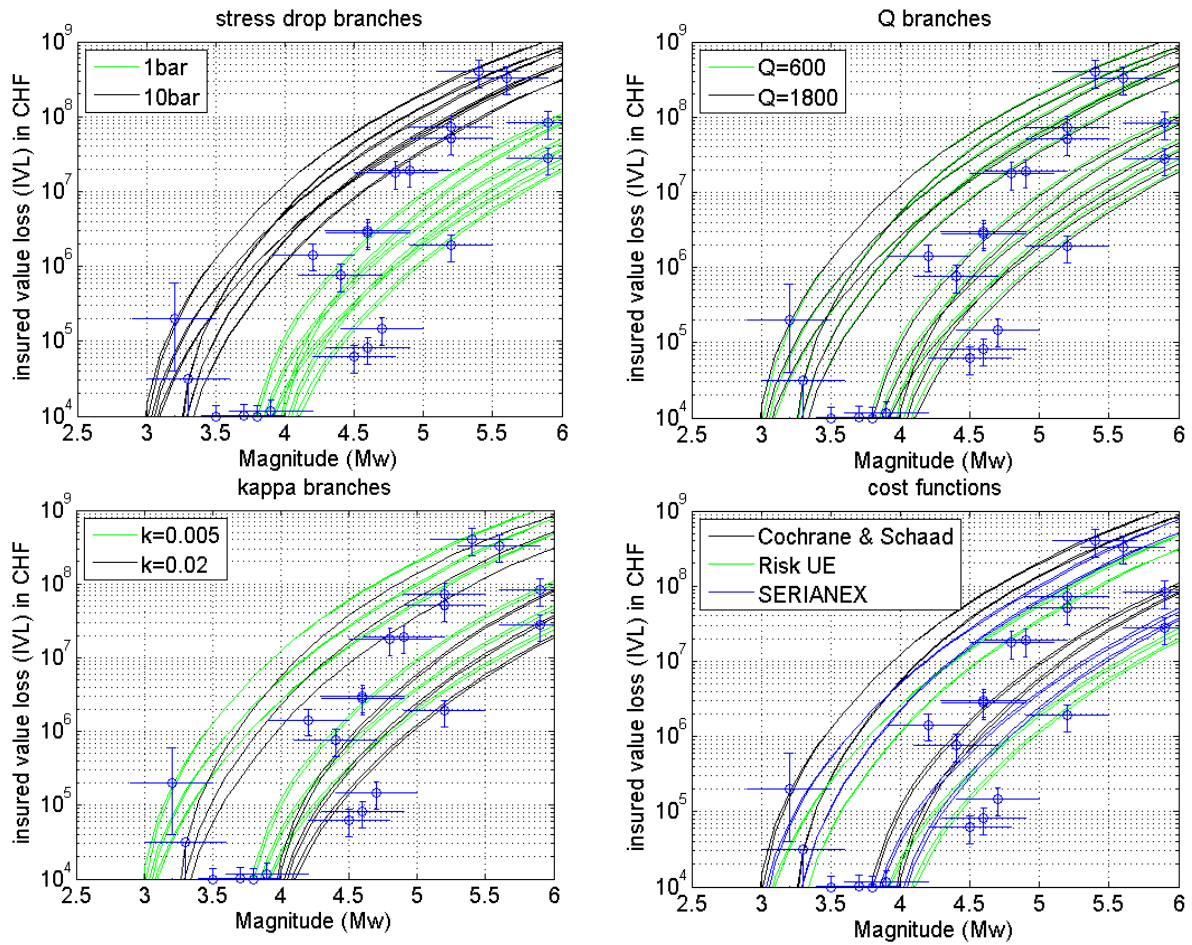


Figure 4: Branches of the tree model color-coded by their constituting parameters. The choice of stress drop is mainly controlling IVL results, whereas the choice of attenuation (Q and κ) has minor effects. Cost functions lead to a difference in IVL by about an order of magnitude.

Results are most sensitive to the selection of stress drop and to a lesser degree to the choice of cost functions. Here the choice of stress drop of 1 bar and 10 bar (0.1 MPa to 1 MPa), results in two clear distinguishable groups of curves and to a factor of 20-100 difference in IVL. The choice of crustal attenuation (Q) has no effect, the site specific attenuation term (κ) only affects IVL in the lower part of magnitudes. Cost functions lead to a spread of loss estimates by approx. a factor of 10.

Aleatory variability

Aleatory variability accounts for the randomness in a process. It is therefore introduced in detail in the framework of the probabilistic risk assessment in chapter 4.1

3.4 Comparison to three earthquake scenarios in the surroundings or within Switzerland

To better illustrate the bandwidth of the 8x3 deterministic models, three events are chosen, that cover most of the epistemic uncertainty (favorable to very unfavorable site and amplification effects).

Sargans, Dec. 12th 2013, Mw=3.8:

The most recent earthquake in Switzerland above Magnitude 4 ($M_L=4.1$) occurred in the Rhine valley, close to the village of Balzers in southern Lichtenstein on 12th Dec. 2013. In the media the event was known as Sargans event. Focal depth is estimated to be $7 \text{ km} \pm 2 \text{ km}$ (Cauzzi et al., 2014) or 5.9 km (website SED). As many people were at rest (the origin time was 00:50 AM UTC), the event was widely felt in the Alpine Rhine valley from Chur towards Lake Bodensee, across Liechtenstein and in adjacent areas of Switzerland and Austria. The station closest to the epicenter registered a pgv of 4 mm/s (Cauzzi et al., 2014). Based on building soil classes and intensity amplification map information, site conditions can be considered as equal or worse compared to the location of Haute-Sorne. For the Sargans event, no damages were reported ($IVL=0$), confirmed by the 'Kantonale Gebäudeversicherungsanstalt'.

Vallorcine Sept. 8th, 2005, Mw=4.5:

On September 8th, 2005 a moderate Mw 4.5 (ML 4.9) earthquake occurred in Vallorcine in the north-western Alps midway between Chamonix (France) and Martigny (Switzerland). The hypocenter was located at 4.3 km below sea level. Though widely felt, it produced only slight damage in the epicentral zone, with a maximum intensity of V on the EMS-98 scale (BCSF 2005; Cara et al. 2007). Site conditions can be considered to be more favorable compared to Haute-Sorne. The buildings in Vallorcine and the surroundings are built on non-amplifying soil according to the intensity amplification map of Kästli et al., 2008.

Epagny, Jul. 15th 1996, Mw=5:

An earthquake occurred on the 15th of July 1996 in the vicinity of the city of Annecy in the French Alps. The earthquake reached a magnitude of ML=5.3, at shallow depths of 1-3 km. Directivity effects were observed and in combination with sedimentary deposits an amplification of ground motion up to factor 8 was observed (Thouvenot et al., 1998). Accordingly losses totaled to a damage of 300 Mio. Francs (Davidovici, 1996), which translates to ~56 Mio CHF nowadays. The moderate to serious damage in the Annecy area is consistent with intensities of VII-VIII. Compared to Haute-Sorne, site effects can be considered as extreme.

Generally, observed damage caused by earthquakes can differ significantly (Figure 2). When comparing predicted damage to the 3 presented events, the first 2 events (Sargans & Vallorcine) would be overpredicted by the best estimate, whereas the last (Annecy-Epagny) would be underpredicted. However, all events despite their significant difference in ground response are captured within the 1 sigma bound of all hazard curves.

3.5 Discussion & Conclusion

In chapter 2.1 it has been shown, that loss data from known earthquakes is well covered within the 1σ of assumed physical realities. Therefore, it will be likely, that despite the unknown response of the underground in Haute-Sorne, the observed damage of an earthquake of magnitude $M_w=4$ or $M_w=5$ will fall in between the 1σ estimate. Only after more data has been collected, e.g. by a stimulation test, epistemic uncertainty can be reduced and the bandwidth of IVL can be narrowed down.

As mentioned in recommendation 1 of the Swiss Seismological Service (SED), the presented scenarios are very unlikely. Up to date no induced earthquakes above $M_w>3.7$ were observed worldwide in the context of enhanced Geothermal Systems (EGS).

Therefore, to judge the potential risk of the presented scenarios it is important, to link earthquake scenarios to their probability of occurrence (Chapter 4).

4 Probabilistic Risk (recommendation 2 of the Swiss Seismological Service)

Recommendation 2:

We suggest that the results for seismicity-rate forecasts, ground motion predictions and estimated losses presented in the report are combined into comprehensive probabilistic hazard and risk curve. These would show the (annualized) exceedance probability as a function of ground motions and a suitable risk measure (building damage degree, financial losses).

To estimate seismic risk, the deterministic estimates of insured value loss (chapter 3) are combined with their probability of occurrence. Using the novel approach of Mignan et al., 2015 aleatoric variability of intensities are combined with epistemic uncertainty using a logic tree approach. The degree of variability is crucial to the outcomes of the method. However, due to lack of empirical studies in the field of induced seismicity, it is yet unclear how much aleatoric variability has to be accounted for. As a consequence results for a variability of ± 1 and ± 2 intensity units are presented. A plot of intensity variations of the Basel and St. Gallen geothermal projects is shown in Figure 5.

Once after down-hole conditions are better constrained (e.g. obtained during a safe pre-stimulation-test) one can give a more accurate forecast to what will happen or how much seismicity can be expected in total. Therefore emphasis is put on the stimulation of a first fracture, as during project phase further actions will be based on the outcome of this stimulation. Nonetheless a total risk estimate (30 fractures) is also presented.

4.1 Input

Magnitude frequency distributions are taken from the synthesis report submitted to the Canton Jura². Distributions are either based on Baisch, 2014 (scientific report E4³, denoted as deterministic study in Figure 1) or based on the method of Gischig & Wiemer, 2013 (scientific report E5⁴, denoted as probabilistic study in Figure 1) extrapolated to a maximum amplitude of Mw=5 and Mw=6.

To account for the natural randomness of intensity measures, a standard deviation of the aleatory variability of 0.93 intensity units (1σ) is assumed. It is the quadratic mean of the sigma of ground motion prediction equations ($\sigma=0.6$) and the sigma of the ground motion intensity conversion equation ($\sigma=0.71$).

Aleatoric variability is assumed to have a Gaussian distribution, however with a cut off at lower and higher ends to exclude unrealistic physical conditions. As the presented loss results depend significantly on the choice of cut off values (e.g. Table 2), all results in this study are presented for cut off values of one and two intensity units.

To justify the choices of a one and a two intensity unit cut-off, intensity data provided by the SED is plotted for the geothermal projects in Basel and St. Gallen (Figure 5).

In the upper range a 1 sigma cut off (+1 intensity unit) is an upper bound for 88 out of 90 observations regarding the Basel Mw=3.2 event and all observations of the Mw=3.3 St. Gallen event, both for epicentral distances <20 km. On the lower end 1 data point is outside the 1 intensity bound for the Basel case, whereas 8 data points do not fall within 2 intensity bounds in the case of St. Gallen.

Based on the choice of epistemic ground motion predictions and the comparison to empirical data an upper aleatoric variability of +1 intensity unit seems reasonable, however towards low observed intensities (I to III) a 2 or even 3 sigma cut off is the better choice. As a two sigma bound is generally accepted within the methodology of probabilistic risk assessment, later results are presented for a variability of ± 1 and ± 2 intensity units.

² Geo-Energie Suisse AG: Synthèse des études relatives à la sismicité induite

³ Q-con GmbH: Bewertung des seismischen Risikos durch ein EGS Projekt in der Gemeinde Haute-Sorne; Hauptuntersuchung

⁴ Geo-Energie Suisse AG: Probabilistic seismic hazard analysis of a geothermal project in the Haute-Sorne community

VERTRAULICH

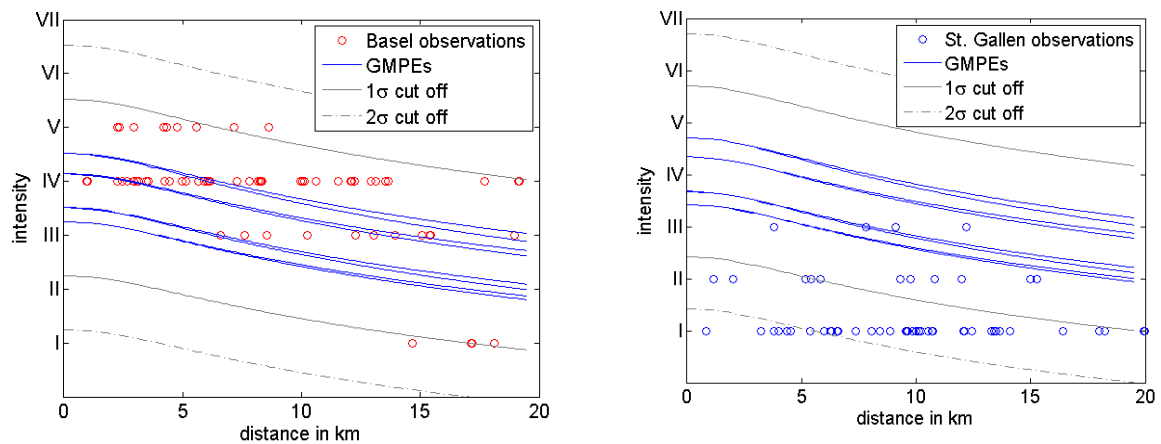


Figure 5: Shown is intensity data within a distance of 20 km for the strongest observed earthquakes of the geothermal projects in Basel (left) and St. Gallen (right). Plotted on top are intensity cut offs of ± 1 and ± 2 intensity units.

4.2 Results and sensitivity analysis to key parameters

Presented in Figure 6 to Figure 8 are best estimates of seismic risk, considered to be the median of all 72 branches of the logic tree approach (Figure 1). Results are shown for 1 and 30 fractures combined with an aleatoric variability of ± 1 and ± 2 intensity units. Further results using a different weighting scheme of branches are shown in Appendix E.

Intensities

To better illustrate the consequences of stimulation, risk is not only expressed as loss of monetary value, but also in terms of exceeding an (epicentral) intensity (Figure 6 & Table 2). Intensities can then be linked to pictures of damage or human perception. For example an event reaching intensity V is felt indoors by most, outdoors by a few people. First non-structural damages generally start occurring at intensity VI (see also EMS98 intensity scale in the Appendix B).

VERTRAULICH

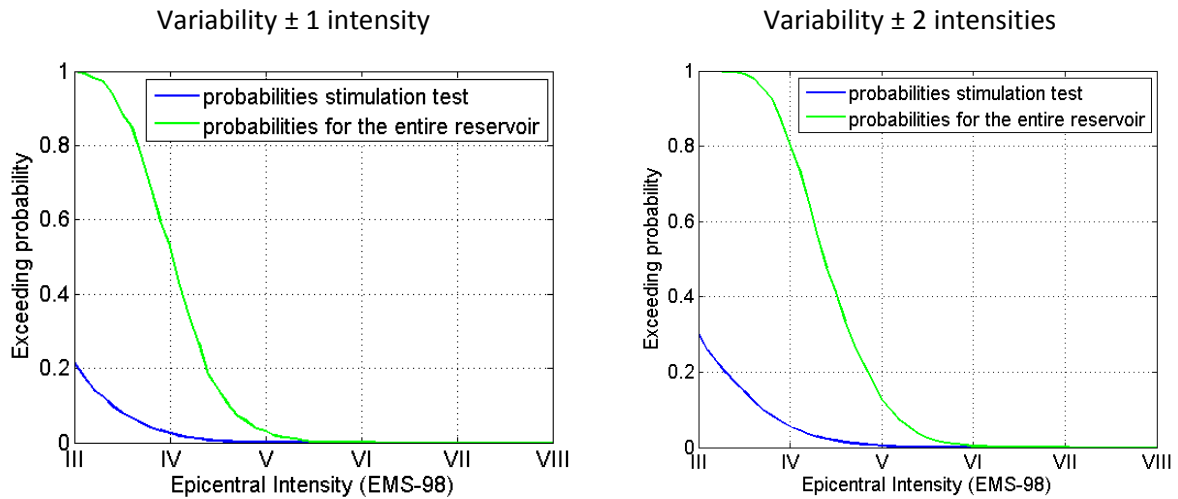


Figure 6: Exceeding probability of epicentral intensity for a variability of ± 1 intensity (left) and ± 2 intensity units (right).

Intensity (EMS 98)	Exceedance probability			
	Variability ± 1 intensity		Variability ± 2 intensities	
	stimulation test	entire reservoir	stimulation test	entire reservoir
IV	2.7%	53%	5.5%	80%
V	0.11%	3.1%	0.4%	12.7%
VI	$1.2 \cdot 10^{-5}$	$6.1 \cdot 10^{-5}$	0.013%	0.38%
VII	$2.1 \cdot 10^{-8}$	$6.3 \cdot 10^{-7}$	$1.4 \cdot 10^{-6}$	$4.3 \cdot 10^{-5}$
VIII	out of physical boundaries		out of physical boundaries	

Table 2: Exceedance probabilities for intensities IV to VII for an aleatoric variability of ± 1 and ± 2 intensity units.

VERTRAULICH

Insured value loss

Shown in Figure 7 & Figure 8 are best estimates regarding the exceedance probabilities of insured value loss, Table 3 lists losses corresponding to selected exceedance probabilities.

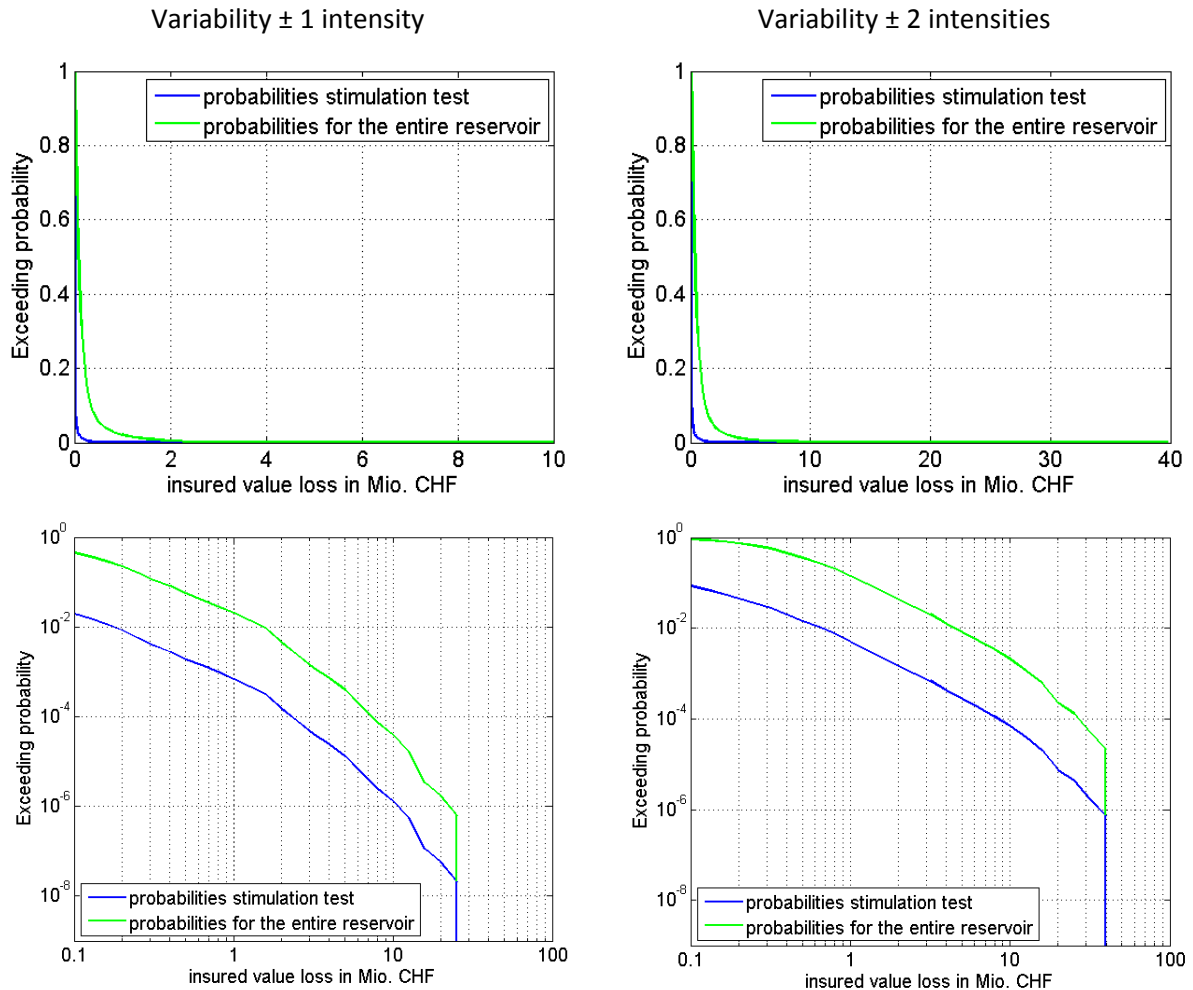


Figure 7: Exceeding probabilities of insured value loss for a variability of ± 1 intensity (left) and ± 2 intensity units (right). Upper row shows probability-loss curves in linear scale, lower row in log scale. All curves have an upper limit for insured value loss, where input becomes unphysical (see last paragraph of this chapter). Therefore, curves are cut when physical boundary conditions are exceeded.

VERTRAULICH

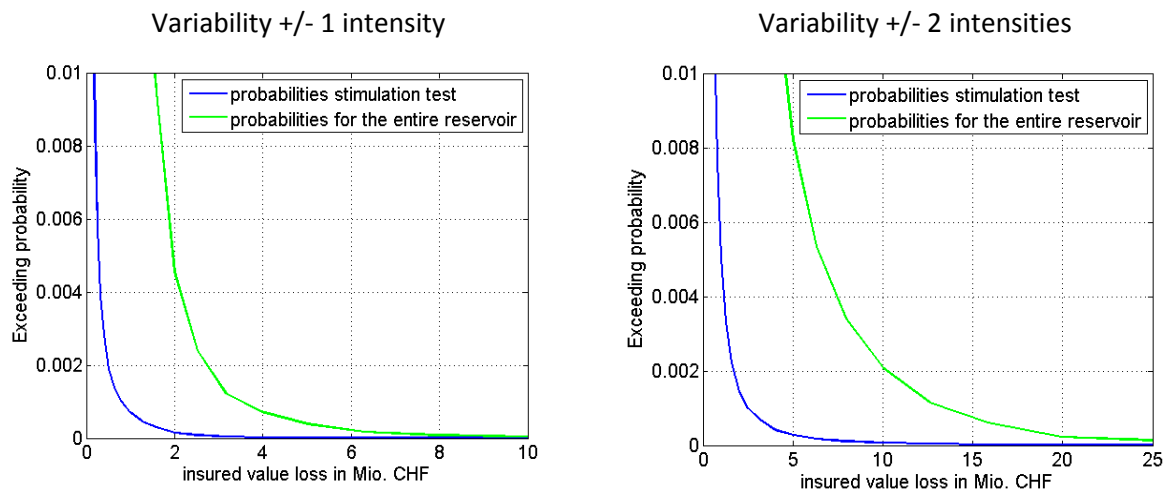


Figure 8: Zoom to curves in Figure 7.

Exceedance probability	Insured value loss			
	Variability ± 1 intensity		Variability ± 2 intensities	
	stimulation test	entire reservoir	stimulation test	entire reservoir
50%	Below resolution of 10'000 CHF	88'000CHF	Below resolution of 10'000 CHF	365'000 CHF
1%	0.18 Mio CHF	1.6 Mio. CHF	0.67 Mio CHF	4.6 Mio. CHF
0.1%	0.79 Mio CHF	3.5 Mio. CHF	2.5 Mio CHF	13.5 Mio. CHF

Table 3: Insured value loss for exceedance probabilities of 50%, 1% and 0.1 %.

All results are calculated using a magnitude frequency distribution (probability of occurrence) that is based on observations during the stimulation of the Basel reservoir. It has been shown by Shapiro et al., 2010 that the seismic response to stimulation (seismogenic index) in Basel is the highest observed among geothermal projects and other fracturing operations in the oil & gas industry.

VERTRAULICH

Weights of the logic tree

Logic tree models are well suited to deal with a large number of physical models and their uncertainties. Using the proposed setup (Figure 1 for IVL and Figure 16 for injuries), model representations of magnitude-frequency distributions, maximum magnitude, ground motion prediction equations and cost functions all add branches to the logic tree. Following Mignan, 2015 all branches are treated equal, however a weighting of branches is usually applied, because some branches are considered less or more likely than others. The choice of weighting parameters is based on expert judgment. In the following, two different weighting schemes are compared (Figure 9 & Figure 10). The first weighting scheme was used in this report and follows Mignan, 2015. This weighting scheme puts double weight on the probabilistic study, because the probabilistic study branch splits into two M_{\max} branches ($M_{\max}=5$ and $M_{\max}=6$), whereas the deterministic part only has one M_{\max} branch ($M_{\max}=3.5$). The second weighting scheme treats probabilistic and deterministic study equally (compare Figure 9 & Figure 10). Be aware, that individual branches remain identical regardless of weighting; however, the best estimate of maximum insured value loss or injuries (Appendix D) changes accordingly.

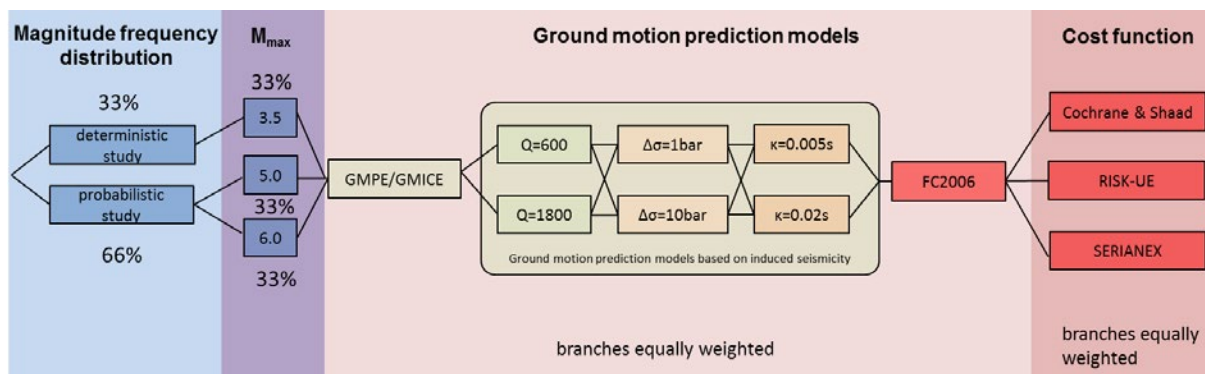


Figure 9: weighting scheme, where all branches have equal weights. Because the probabilistic branch splits into two M_{\max} branches, this weighting scheme put twice the emphasis on the probabilistic study.

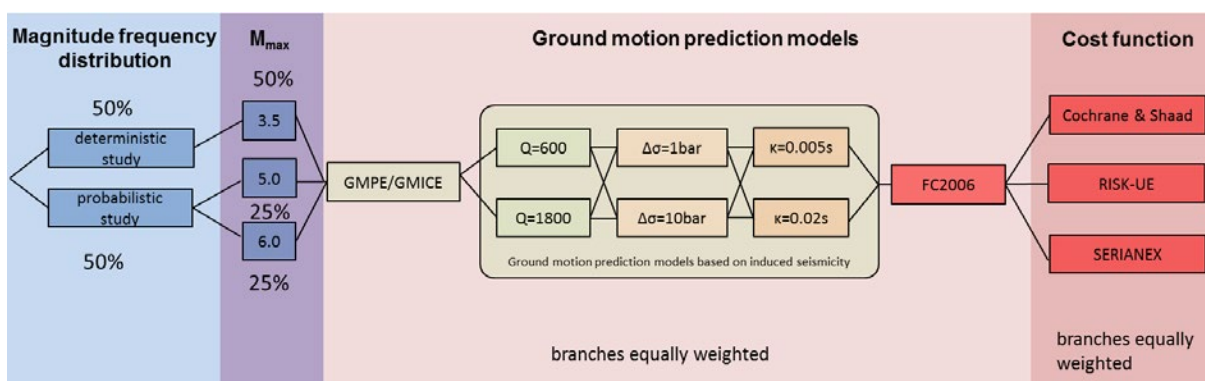


Figure 10: weighting scheme where deterministic and probabilistic studies have equal weights assigned.

VERTRAULICH

In Table 4 & Table 5 we summarize the results and show the influence of weighting on maximum most likely insured value loss and injuries. Note that maximum values are identical for the stimulation test and the stimulation of the entire reservoir and in all cases are below OPAM thresholds (Chapter 5). Additional plots comparing results for different weighting schemes can be found in Appendix E.

Best estimate of max. insured value loss	Variability ± 1 intensity	Variability ± 2 intensities
Weighting Mmax: 0.33 / 0.33 / 0.33	25.1 Mio. CHF	39.8 Mio. CHF
Weighting Mmax: 0.5 / 0.25 / 0.25	4 Mio. CHF	25.1 Mio. CHF

Table 4: Best estimate of maximum insured value loss (IVL) for different weights of the logic tree and different assumptions on aleatoric variability.

Best estimate of max. injuries	Variability ± 1 intensity	Variability ± 2 intensities
Weighting Mmax: 0.33 / 0.33 / 0.33	<4 (3.16)	<4 (3.55)
Weighting Mmax: 0.5 / 0.25 / 0.25	<1 (0.28)	<4 (3.16)

Table 5: Best estimate of injuries for different weights of the logic tree and different assumptions on aleatoric variability (see also Appendix D).

4.3 Discussion

Results are most sensitive to the selection of ground models – in particular the choice of stress drop and the assumption about the statistical variability of intensity observations (Chapter 3.1 & 4.1). Different weighting of individual branches of the logic tree shows a significant influence on maximum values of insured value loss or injuries (Table 5).

In this study the selection of ground motion prediction models covers a wide range of physical realities. The range of models combined with aleatoric variability can lead to extreme cases, which are at the edge of being physically possible. For example using a variability of ± 2 intensity units, combined with the Magnitude $M_w=3.2$ event in Basel, intensities VI to VII are considered possible. In Basel the maximum observed intensity was V. Intensities VI to VII are usually observed for magnitudes $M_w=4.5$ to $M_w=5.5$ (see Appendix B), such earthquakes lead to ground motions being 20-200 times higher compared to a magnitude 3.2 event. Although such scenarios represent the tails of a Gaussian distribution they have a significant impact on results. Based on the argumentation above and for the chosen setup of GMPEs, results for a variability of ± 2 intensity units are probably over conservative, whereas results for a variability of ± 1 intensity unit can be considered to better represent physical site conditions.

Losses are bound by physical constraints. The tectonic setting in the vicinity of Haute-Sorne leads to a maximum magnitude (M_{max}), then via ground motion models to a maximum intensity and consequently to a maximum loss in the models. Hence, best estimates of losses do not exceed 25.1 Mio. CHF at probabilities $< 10^{-6}$ (variability ± 1 intensity unit) and 39.8 Mio. CHF at probabilities $< 10^{-4}$ (variability ± 2 intensity units), respectively. These considerations also explain the kink towards 0 probability in Figure 7.

Results for best estimates of this study were obtained by an equal weighting of all branches, however a weighting of branches is usually applied, because some branches are considered less or more likely than others. The choice of weighting parameters is based on expert judgment. Weighting of branches is also likely to change when the geothermal project progresses and more information becomes available. Ideally some branches can then be excluded and are assigned weight 0. As shown in Table 4 & Table 5 weighting can have a significant impact on maximum values of insured value loss, casualties or injuries.

5 Risk in the framework of OPAM

The risk presentation in the framework of OPAM was added by the request of the Canton Jura. The OPAM is intended to judge risk imposed by chemical plants and contains acceptability criteria regarding casualties and financial losses. The OPAM applies if the number of casualties exceeds 10, or the financial loss is greater than 64⁵ Mio CHF.

⁵inflation and building index corrected value, initially 50 Mio CHF based on building values of 1996

5.1 Casualties

Method

Human casualty estimation follows the method described in Landtwin, 2012. It is based on loss estimation models of QLARM (Earthquake Loss Assessment for Response and Mitigation), Trendafiloski et al., 2011 and STEER (short- Term Earthquake Risk Assessment), van Stiphout, 2009. Both QLARM and STEER use five different damage grades according to HAZUS (1999). Casualty matrices derived from HAZUS are then used to transfer damage information obtained by the deterministic model in Chapter 2 to the number of injured or dead persons.

Results

In all calculations the number of casualties never exceeds 1⁶, therefore no plots are shown. A rule of thumb is that human losses are still unlikely for intensity VII and usually start occurring at intensities of VIII or above. The result of 0 casualties is in agreement with the presented exceedance probability of intensities in Figure 6 and Table 2, where probabilities for intensity VII are less than $4.3 \cdot 10^{-5}$ and intensities of VIII are not reached.

5.2 Financial risk judged by OPAM

In seismology, seismic risk is usually expressed in terms of exceedance probability over a certain time interval, which is a cumulative measure of risk. In this study the time interval was set to the duration of the entire stimulation. The OPAM uses a different terminology in expressing risk. Here risk is given in 'yearly probability', which is an annual cumulative rate of occurrence.

For the stimulation process the one year time interval of OPAM is too long, as the stimulation process will be shorter (approx. half a year). For a conservative OPAM-type estimate of risk it is assumed that the stimulation last exactly one year, however one could scale down risk with the ratio of stimulation time vs. one year. To illustrate the difference in risk measures, Figure 11 shows both measures of risk, exceedance probability and yearly cumulative rate of occurrence in one plot. A short chapter about converting one measure of risk into the other is added in appendix C.

Regardless of the representation of risk, the loss-axis remains unchanged. Best estimates of maximum losses of 25.1 Mio. CHF (variability ± 1 intensity unit) and 39.8 Mio. CHF (variability ± 2 intensity units) remain below the threshold of 64⁷ Mio CHF where OPAM starts to apply (Figure 11).

⁶ The physical boundary of human losses is reached at 0.013 casualties along with an exceeding probability of $1.9 \cdot 10^{-5}$ for a system of 30 fracs and the unfavorable setting of an aleatoric variability of ± 2 intensities.

⁷inflation and building index corrected value, initially 50 Mio CHF based on building values of 1996

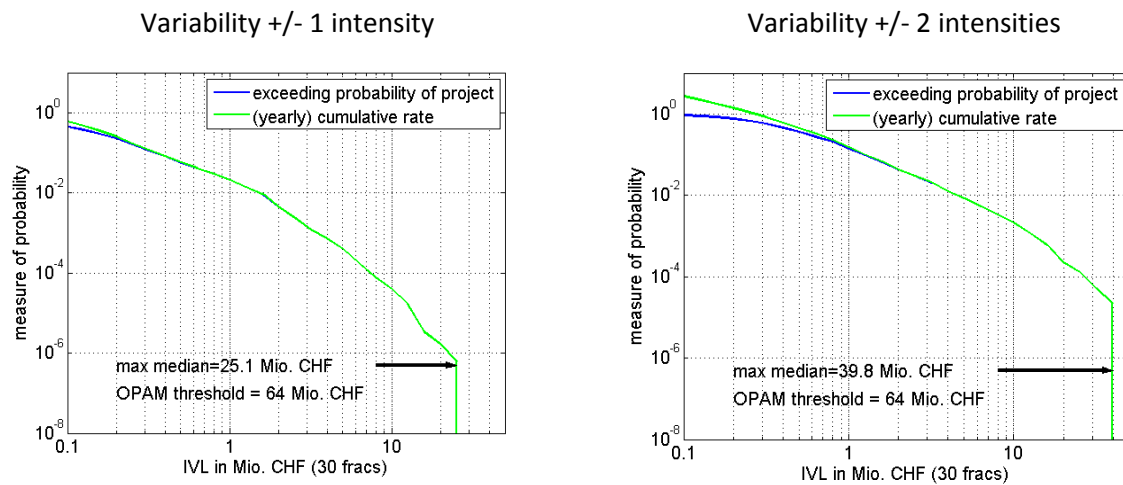


Figure 11: Comparison between exceedance probability and cumulative occurrence rate. Due to physical constraints (Chapter 4.3) best estimates of maximum losses (25.1 Mio. CHF and 39.8 Mio CHF) do not exceed the loss threshold level of OPAM (64 Mio. CHF).

6 Individual risk

In chapter 5.1 it was shown, that the risk of casualties is acceptable when OPAM criteria are applied. However, the representation of the risk of casualties using a double logarithmic scale is difficult to interpret. This is especially true when the risk curve spreads several orders of magnitude and ends at $\sim 10^{-2}$ casualties at an occurrence rate of roughly $\sim 10^{-6}$.

For this reason the risk of casualties is also presented in terms of a single number, the individual risk or potential loss of life. The following procedure picks up suggestions by Blaise Duvernay (BAFU), meaning that the calculation of individual risk is exactly the same as for societal risk, but with only one vulnerable object built on the soil class with highest amplification potential in the area. As suggested by Duvernay, the integration of the median risk curve then leads to the desired probability estimate. Following the suggestions, the median of risk curves (based on magnitude-frequency distribution, Mmax and ground-motion prediction equations) is coupled with a number of pessimistic assumptions (Table 6 & Figure 12) and then integrated to obtain individual risk. The choice of parameters yields to a reasonable upper bound of risk, therefore statistical (aleatory) variability is not considered. Later it will be demonstrated, that the conservative choice of parameters leads to a higher risk compared to a most likely parameter approach with a high variability (2σ).

6.1 Method

Similar to the method described in Chapter 5.1, individual casualty estimation is based on a logic tree approach using loss estimation models of QLARM and STEER. The vulnerability index of a building leads to an EMS-98 vulnerability class resp. to a QLARM collapse probability. Using casualty

VERTRAULICH

matrices derived from HAZUS then lead to a probability of surviving or dying due to an earthquake of a certain magnitude or seismic intensity, respectively.

The probability of dying can then be coupled with the (annual) probability of occurrence of earthquakes (intensities) induced by the geothermal project.

For the calculation of individual risk both probabilities then need to be combined to one single value. Yet, there is not a best practice how individual risk should be computed. Jonkman et al., 2003 list about 25 quantitative risk measures how such computations can be made. Here we choose a method, which we consider the most reasonable, using the statistical expectancy value, in literature often referred to as the potential loss of life (PLL):

$$PLL = \int_0^{\infty} x f_N(x) dx,$$

where $f_N(x)$ is the continuous probability density function for the chance of dying and x the occurrence rate (Ale et al., 1996).

Using the logic tree method, each branch leads to one value of individual risk. Of all (conservative) branches (Figure 12), the median is taken as best conservative estimate. Calculation is done for 30 stages, which is a multiplication of individual risk by a factor of 30 compared to a single stage and by itself is also a conservative assumption (Alcolea & Bethmann, 2013).

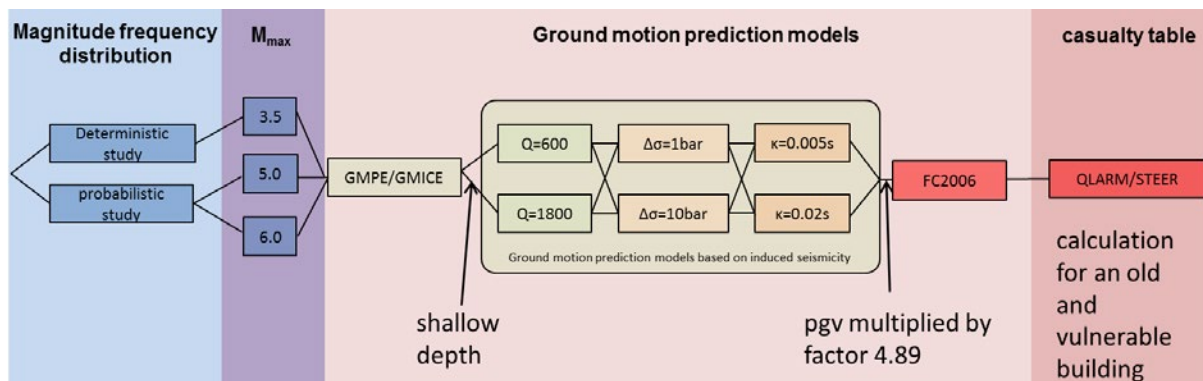


Figure 12: logic tree to calculate individual risk, shown are changes for a pessimistic case. In analogy to Figure 9 and Figure 10 different weighting schemes can be applied

6.2 Input

Magnitude-frequency distributions and ground motion prediction equations are the same as used for the calculation of insured value loss, injuries or casualties in previous chapters. The logic tree is shown in Figure 12. Ground motion predictions and injury/casualty tables are then coupled with pessimistic parameter choices (Table 6 and Figure 12). The building stock is reduced to a very old and vulnerable house.

VERTRAULICH

The conservative case was defined upon approval by experts of the Swiss Seismological Service; details are described in Table 6:

- A person spends 24h per day in a very old house,
- the house is vulnerable to ground shaking and
- sits on a highly amplifying ground.
- The earthquakes are happening directly underneath the building at shallow depth (3.5km).

topic	Most common or typical value	pessimistic assumption
time spent in house	16 hours estimated using statistics of the US bureau of labour statistics http://www.bls.gov/news.release/atus.t12.htm	24 hours
age of house and vulnerability	Built after 1946, building class M3 or better, falling into the V ₀ category, vulnerability index is 0.62 or lower, EMS-98 vulnerability class C	Built before 1919, building class M1, falling into the V+ category, vulnerability index 0.83, EMS-98 vulnerability class B
ground motion amplification	Amplification using soil class C: 2.79*pgv, or intensity based on intensity amplification map: $\Delta I = +0.47$	Amplification using soil class E: 4.89* pgv (most conservative), or intensity based on intensity amplification map: $\Delta I = +0.72$
Distance to earthquake	4.5km average depth heat exchanger, hypocentral distance is usually larger as most buildings will not be situated on top of heat exchanger	3.5 km top of heat exchanger -175m.
Stimulation procedure	30 stages, learning effect and 'stress shadowing' lead to a reduced risk for stimulation of subsequent stages – up to date such effects are not yet considered	30 stages, no learning curve, risk of one stage is multiplied by 30
Stimulation time	Less than a year (1/2 year at current planning stage)	1 year

Table 6: comparison of most common values of parameters vs. pessimistic assumptions

6.3 Results

The individual risk, defined as best estimate (median) of conservative risk models, for a stimulation of 30 stages equals to $9.5 \cdot 10^{-9}$ using an equal weighting of branches (Figure 9). 1σ bounds of the

VERTRAULICH

total risk distribution, defined as 68% of the branches around the median, are at $1.9 \cdot 10^{-11}$ and $1.0 \cdot 10^{-6}$.

In case an equal weighting of risk studies is chosen (Figure 10), the best estimate (median) of risk is $3.1 \cdot 10^{-9}$. 1σ bounds of the total risk distribution are at $1.8 \cdot 10^{-11}$ and $9.5 \cdot 10^{-7}$.

Following the suggestions by Duvernay, the presented median values for individual risk are taken as a best estimate for a reasonable pessimistic case. However, it is always possible to find more conservative/pessimistic estimates (see discussion). The way individual risk is calculated in this chapter, is more conservative than calculating risks in previous chapters, where a most reasonable setup was chosen and 1 or 2 intensity units for aleatory uncertainty were incorporated. To compare both methods, individual risk is also calculated choosing a typical setup (Table 6) and adding an aleatory variability of 2 intensity units. The individual risk is lower compared to the pessimistic case and sums up to a probability of $5.0 \cdot 10^{-10}$ for an equal weighting of branches, or $2.3 \cdot 10^{-10}$ for an equal weighting of risk studies. 1σ bounds are $[5.5 \cdot 10^{-12}; 2.7 \cdot 10^{-8}]$ and $[4.7 \cdot 10^{-12}; 2.2 \cdot 10^{-8}]$, respectively.

6.4 Discussion

Jonkmann et al, 2003 show a collection of acceptance limits for individual risk that are applied worldwide. Quite indulgent limits are listed for dams in the US or Canada of 10^{-2} and 10^{-3} , respectively. The strictest criteria are applied in the Netherlands and UK at 10^{-6} , which seems to become a commonplace in public health discourse and policy (e.g. Cornwell & Meyer, 1997 for a summary). The individual risk for the stimulation activity for the geothermal project in Haute-Sorne, defined as the median of a suite of pessimistic models, is lower by at least a factor of 100 ($\sim 10^{-8}$).

The computation of individual risk is based on reasonable pessimistic assumptions, which are reviewed by experts of the Swiss Seismological Service. It is not useful to push parameter settings further to the extreme. For the modeled house it is already unclear if such a building exists in the community of Haute-Sorne. Given the fact, that old city centers are usually built on 'safe' ground, vulnerable buildings built on the highly amplifying soil class 'E' might not even exist. This fact can be confirmed by a map study⁸ that shows, that the city centers of the surrounding communities Bassecourt, Berlincourt, Glovelier and Boécourt are either built on class 'A' or 'C', but not on the highly amplifying class 'E'. However, boundaries on maps are not strict and sometimes contradicting and therefore class 'E' was chosen.

The reasoning about the conservative choice of other parameters is similar. Usually Swiss building stock has a good quality. In particular the Canton Jura is known for using fairly good rocks compared

⁸

http://map.geo.admin.ch/?X=243405.78&Y=583133.87&zoom=7&lang=de&topic=ech&bgLayer=ch.swisstopo.pixelkarte-farbe&catalogNodes=457,532,477,533,567,583&layers_opacity=0.75&layers=ch.bafu.gefahren-baugrundklassen

VERTRAULICH

to other regions in Switzerland (SED pers. comm.), yet a high building vulnerability was chosen. - The time of stimulation is currently estimated to last half a year, one year was chosen for calculation, etc.

It is also not advisable to pick the most conservative branch out of the logic tree, because it opposes the philosophy of a logic tree. The purpose of a logic tree is to incorporate different model views, which may be supported but also may be disputed by experts. A focus on one branch therefore would contradict the mindset of the logic tree being mutually exclusive and cumulatively exhaustive. At a later stage of the project, when more information is available, higher or lower weighting of branches will be applied based on measurements. With the gain of knowledge, individual risk will then be recomputed. To give an impression of the current variety of results 1σ bounds of the total risk distribution, defined as 68% of the branches around the median were also presented.

Summarizing, by the choice of parameters, the presented individual risk can be considered as a reasonable upper bound. The individual risk of $\sim 10^{-8}$ is low compared to other risks posed by industry (Hess, 2006).

7 Conclusion

We present a probabilistic seismic risk analysis for the geothermal project in the community of Haute-Sorne. The analysis is based on recommendations of the Swiss Seismological Service and additional requests of the Canton Jura after the submission of the main investigation of the environmental impact assessment. Using a logic tree approach, we calculated a best estimate of insured value loss as well as potential casualties and individual risk. In addition the sensitivity of risk estimates to different input parameters was investigated. Uncertainties at the hazard and risk levels were considered in a systematic way in the scope of induced seismicity regimes. We show that the chosen models cover a broad range of physical underground conditions and can explain well observations for other induced or natural events.

Currently, at the geothermal site, the seismic response to underground stimulation is unknown; therefore the high seismic response of the Basel underground was taken as proxy. Once information obtained by a stimulation test becomes available, the current study can be updated and adapted to downhole conditions. It is expected, that both epistemic uncertainty (the number of physical realities) and aleatoric variability (the natural randomness) will reduce with the gain of data. Some branches of the logic tree can then be eliminated and randomness of intensity observations can be narrowed down by observations and immission analysis.

In the case of the Basel geothermal project, risks were compared against permissible values for industrial constructions that can pose significant risks to health and environment (StFV or OPAM). The consultation of OPAM applies, whenever more than 10 casualties or a financial loss of 64⁹ Mio

⁹inflation and building index corrected value, initially 50 Mio CHF based on building values of 1996

VERTRAULICH

CHF is exceeded. The OPAM is the only regulation which gives an acceptability criterion for financial losses in addition to casualties.

Regarding maximum financial loss, the best estimate (Figure 7) is restricted to 25.1 Mio. CHF at probabilities $< 10^{-6}$ (variability ± 1 intensity units) and 39.8 Mio. CHF at probabilities $< 10^{-4}$ (variability ± 2 intensity units), respectively. The presented losses remain below the threshold where OPAM starts to apply. Higher losses are considered to be unphysical, because losses are constrained by a maximum magnitude / intensity value. Therefore, the risk is also acceptable in terms of financial loss.

Regarding casualties, the presented risk using OPAM criteria, is certainly acceptable. The number of casualties for the geothermal project does not exceed ~ 0.01 on the OPAM log-log plot. However, a fraction of a casualty is not very meaningful; therefore risk of casualties is expressed in terms of individual risk.

As a general rule of thumb, potential loss of life due to technical risks should be a factor 10 less compared to natural hazards. A strict limit worldwide is 10^{-6} but could also be as low as 10^{-2} (Jonkmann, 2003). In case of the geothermal power plant in Haute-Sorne, individual risk calculated using reasonable pessimistic assumptions leads to values that are approximately 10^{-8} . This is 100 times lower than the strict limit of 10^{-6} .

We conclude with a statement of the Swiss Seismological Service cited in the evaluation report of the main environmental impact assessment study:

“It is a fact, that deep geothermal energy projects have so far caused neither structural damages nor harmed people”.

The risk study confirms what is observed worldwide for deep enhanced geothermal projects.

8 References

Alcolea, A., Bethmann, F., 2014 *Probabilistic seismic hazard analysis of a geothermal project in the Haute-Sorne community*.

B.J.M. Ale, G.M.H. Laheij, P.A.M. Uijt de Haag, Zoning instruments for major accident prevention, in: C. Cacciabue, I.A. Papazoglou (Eds.), *Probabilistic Safety Assessment and Management, ESREL 96—PSAM-III*, Crete, 1996, p. 1911.

Baisch, S., Carbon, D., Dannwolf, U., Delacou, B., Devaux, M., Dunand, F., Jung, R., Koller, M., Martin, C., Sartori, M., 2009. *Deep Heat Mining Basel: Seismic Risk Analysis*, SERIANEX Group. Departement für Wirtschaft, Soziales und Umwelt des Kantons Basel-Stadt, Basel.

Baisch, S., Vörös, R., Pulm, P., 2013, *Bewertung des seismischen Risikos durch ein EGS Projekt in der Gemeinde Haute-Sorne: Hauptuntersuchung*, Version 131223, GEOS005

BCSF (2005) *Séisme de Vallorcine (Savoie) du 8 Septembre 2005. Note préliminaire* BCSF2005-NP4. BCSF, Université de Strasbourg.

http://www.franceseisme.fr/donnees/intensites/2005/050908_1127/050908_NotePrel_Vallorc_Part1.pdf. Accessed 11 March 2010

Cara M, Schlupp A, Sira C (2007) *Observations sismologiques: sismicité de la France en 2003, 2004, 2005*. Bureau Central Sismologique Français, ULP/EOST – CNRS-INSU, Université de Strasbourg

Cochrane, S., Shaad, W., 1992. *Assessment of earthquake vulnerability of buildings*. In: Paper presented at Earthquake Engineering, 10th World Conference, Balkema, Rotterdam. Douglas, J., Edwards, B., Convertito, V., Sharma, N., Tramei, A., Kraaijpoel, D., Mena Cabrera, B., Maercklin, N., Troise, C., 2013. Predicting ground motion from induced earthquakes in geothermal areas. *Bull. Seismol. Soc. Am.* (accepted February 2013).

Cornwell, J.B., Meyer, M.M., 1997 Atil risk control seminar Petróleos de Venezuela, Puerto de la Cruz, *Risk acceptance criteria or 'How safe is safe enough'?*

Davidovici, V. 1996: *Le séisme du 15 juillet, au Nord d'Annecy*. In: Le Séisme d'Epagny (Haute-Savoie, France) du 15 juillet 1996. Rapport de la mission AFPS. Association Française du Génie Parasismique, Paris, p 99-127.

Fäh, D., Giardini, P., Kästli, N., Deichmann, M., Gisler, G., Schwarz-Zanetti, S., Alvarez-Rubio, S., Sellami, B., Edwards, B., Allmann, F., Bethmann, J., Wössner, G., Gassner-Stamm, S., Fritsche, D., Eberhard, (2011). *ECOS-09 Earthquake Catalogue of Switzerland Release 2011. Report and Database. Public catalogue*, 17.4.2011. Swiss Seismological Service ETH Zürich, Report SED/RISK/R/001/20110417.

Facciolo, E., Cauzzi, C., 2006. *Macroseismic intensities for seismic scenarios, estimated from instrumentally based correlations*. In: 1st European Conf. Earth-quake Engineering and Seismology, 3–8 September 2006, Geneva, Switzerland, p. 569.

Fäh, D., Giardini, D., Bay, F., Bernardi, F., Braunmiller, J., Deichmann, N., Furrer, M., Gantner, L., Gisler, M., Isenegger, D., Jimenez, M.J., Kästli, P., Koglin, R., Masciadri, V., Rutz, M., Scheidegger, C., Schibler, R., Schorlemmer, D., Schwarz-Zanetti, G., Steimen, S., Sellami, S., Wiemer, S., Wössner, J., 2003. *Earthquake Catalogue Of Switzerland (ECOS) and the related macroseismic database*. *Eclogae Geol. Helv.* 96, 219–236, <http://dx.doi.org/10.1007/s00015-003-1087-0>.

Grünthal, G., R.Wahlström, and D. Stromeyer (2009). *The unified catalogue of earthquakes in central, northern, and northwestern Europe (CENEC)* —updated and expanded to the last millennium, J. Seismol. 13, 517–54, doi [10.1007/s10950-008-9144-9](https://doi.org/10.1007/s10950-008-9144-9).

Genoni, O., Ebert A., Häring C., 2012 *Schadenssynthese Basel*, Projektauftrag PA 8-6 für Geo-energie Suisse AG

Gischig, V. S., Wiemer S. (2013). *A stochastic model for induced seismicity based on non-linear pressure diffusion and irreversible permeability enhancement*. Geophysical Journal International, doi:10.1093/gji/ggt164.

Goertz-Allmann, B.P, Edwards, B., Bethmann, F. Deichmann, N. Clinton, J. Fäh, D., Giardini, D., *A new empirical ,magnitude scaling relation for Switzerland*, BSSA, 2011, Vol. 101, No.6, pp. 3088-3095

HAZUS (1999), *HAZUS 99 Technical Manual*, in Federal Emergency Management Agency, edited, Washington, D.C.

Hess. J. Th., *Schutzziele im Umgang mit Naturrisiken in der Schweiz*, 2006, vdf Hochschulverlag AG (S.43 Tabelle 20)

Jonkmann, S.N., van Gelder, P.H.A.J.M., Vrijling, J.K., *An overview of quantitative risk measures for loss of life and economic damage*, Journal of hazardous materials A99, 2003, 1-30

Kästli, P. Fäh, D. 2008 *Site amplification factors for intensity attenuation ; a case study for Switzerland*, submitted to natural hazards

Landtwing, D., 2012, *towards real-time probabilistic seismic risk assessment of induced seismicity for future Swiss enhanced geothermal projects, master thesis, Department of earth sciences, Swiss Seismological Service, ETH Zürich*

Mignan, A. Landtwing, D., Kästli, P. Mena, B. Wiemer, S. ,2015. *Induced seismicity risk analysis of the 2006 Basel, Switzerland, enhanced Geothermal System project: Influence of uncertainties on risk mitigation*, Geothermics53 (2015), 133 -146 (available online)

Mouroux, P., Le Brun, B., 2006. *Presentation of RISK UE Project*. Bull. Earthquake Eng.4, 323–339, <http://dx.doi.org/10.1007/s10518-006-9020-3>.

Thouvenot, F., Fréchet,J., Tapponnier, P. Thomas,J.C., Le Brun, B., Ménard G., Lacassin, R., Jenatton, L., Grasso, J. R., Coutant, O., Paul, A., Hatzfeld D., 1998, *The ML 5.3 Epagny (French Alps) earthquake of 1996 July 15 : a long awaited event on the Vuache fault*, Geophys. J. Int, 135, 876-892

Shapiro, S., Dinske, C. Langenbruch, C., Wenzel, F. 2010, *seismogenic index and magnitude probability of earthquakes induced during reservoir fluid stimulations*, the leading edge, March 2010, special section microseismic, pp 305-308

Trendafilovski, G., Wyss, M. Rosset, P., 2001, *loss estimation module in the second generation software QLARM, human casualties in earthquakes*, edited by R. Spence, E. So and C. Scawthorn, pp 95-106, springer, Netherlands

Van Stiphout, T. , 2009, *Uncertainty assessment in statistical seismology applications to subduction zone processes and time-dependent hazard and risk*, Dissertation, Eidgenössische Technische Hochschule ETH Zürich. Nr 18487. 2009

VERTRAULICH

Appendix

A. Empirical data

A.1. List of earthquakes and sources

Date	Site	Magnitude	Depth	Damage (IVL)	Injuries / deaths	source
1951	Euskirchen	Mw=5.1	9 km	65 Mio. DM	11/-	Gfz, Wikipedia & ⁽¹⁾
1970	Albstadt	Mw=4.9	8 km	1 Mio. DM	-/-	Gfz & ⁽¹⁾
1975	Sünna	ML=5.2	1 km	3 Mio. DM	3/-	⁽¹⁾
1978	Ebingen	ML=5.7	7 km	275 Mio. DM	23/-	Stuttgarter Nachrichten
1989	Völkershäusen	Mw=5.6	1 km	40.5 Mio. DM	6/-	Wikipedia
1991	Vaz (Graubünden)	Mw=4.7	6 km	Some fissures observed	-/-	SED website
1992	Roermond	Mw=5.4	18 km	160 Mio. DM	30/-	Gfz & ⁽¹⁾ & Wikipedia
1992	Buchs	Mw=4.3	2 km	little dmg. crumbling of plaster	-/-	SED
1996	Annecy	ML=5.3	1-3 km	300 Mio. Francs	1/-	Thouvenot et al., 1998 & ⁽²⁾
2004	Rotenburg	ML=4.5	5 km	61 dmg. claims	-/-	BGR
2004	Waldkirch	ML=5.2	9 km	10 Mio. €	-/-	Gfz & Augsburger Allgemeine
2005	Vallorcine	Mw=4.4	4 km	Dmg. cat. 1 in 18 villages	1/-	BCSF, Observations sismologiques 2003-2005
2006	Basel	ML=3.4	4.7 km	3-9 Mio CHF	-/-	Deichmann & Giardini, 2009 & ⁽³⁾
2008	Neunkirchen	ML=4.5	1 km	17 Mio €	-/-	Gfz & Saarbrücker Zeitung, Zeit.de
2009	Buchs	ML=4.1	10 km	-	-/-	Website SED, www.news.ch , kantonale Gebäudeversicherung
2011	Goch	Mb=4.6	3 km	-	-/-	Gfz & www.goch.de , rp-online.de
2011	Bad Ems	Mw=4.4	12 km	Tilted	-/-	Gfz & ntv.de

VERTRAULICH

				chimeys, 70 houses damaged		
2011	Lorca	Mw=5.1	2-5km	100-575 Mio. CHF 492 Mio. CHF most likely	300/9	USGS / EMSC & ⁽⁴⁾ Consorcio de compensacion de seguros
2012	Emilia Romagna 1	Mw=6.1	9 km	127 Mio \$	50/7	Wikipedia & ⁽⁴⁾
2012	Emilia Romagna 2	Mw=5.8	7.5 km	508 Mio \$	350/17	Wikipedia & ⁽⁴⁾
2012	Zug	ML=4.2	30 km	-	-/-	Website SED, kantonale Gebäudeversicherung
2013	St. Gallen	ML=3.5	5 km	100'000 CHF goodwill payment	-/-	Website SED, pers. Comm / www.srf.ch
2013	Sargans	ML=4.1	5.9 km	-	-/-	Website SED, kantonale Gebäudeversicherung

Table 7: List of earthquakes and sources.

⁽¹⁾ Naturkatastrophen in Deutschland, Schadenerfahrungen und Schadenpotentiale, Münchener Rückversicherungs-Gesellschaft, 1999

⁽²⁾ N. Deichmann, 2012 Earthquakes in Switzerland and surrounding regions 1996-2011, Swiss seismological service-ETH Zürich,

⁽³⁾ Genoni, et al., 2012 Schadenssynthese Basel, Projektauftrag für Geo-Energie Suisse AG

⁽⁴⁾ CATDAT damaging earthquake database 2012- the year in review, rev v5

A.2. Corrections and conversions

Magnitude conversion:

As a common magnitude for comparison, moment magnitude (Mw) is chosen. Whenever possible, magnitude information was taken either from the Geoforschungszentrum Potsdam (Geofon) or the Swiss Seismological Service (ECOS 2009 catalogue or website). In case only local magnitude information was available, MI was converted into Mw for Swiss data after Allmann et al., 2011 or Grünthal et al., 2009 for data outside Switzerland. An uncertainty of 0.3 magnitude units is assumed to incorporate the various sources of information and different conversion equations.

VERTRAULICH

Currency conversion:

For conversion of foreign and/or outdated currencies into Swiss francs a web tool was used (unitjuggler.com). A 40% uncertainty is added to incorporate inflation and fluctuating exchange rates.

Population density correction

The population density correction accounts for the fact, that losses will be higher in denser populated areas. It is assumed that damages scale linear with population density. Two radii of investigation are defined. For earthquakes with $M_w < 3.5$ the population density within a radius of 12 km is used, for earthquakes with $M_w \geq 3.5$ a radius of 20 km is defined. Losses in this study are scaled to the population density of the community of Haute-Sorne within 12 km & 20 km around the center of the planned heat exchanger.

Magnitude -depth correction

Literature data for damages of (induced) earthquakes contain 3 different pieces of information: magnitude, depth and damage. To make data comparable magnitude and damage have to be compared for earthquakes at a common hypocentral depth/ equal distance to building stock.






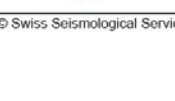

For comparison a common depth of 5 km is chosen, which is a typical depth for induced seismicity within the heat exchanger. Then, in a forward modeling type approach, the damage for a range of magnitudes at 5 km depth is determined, until the calculated damage matches the literature value.

A summary of population and magnitude-depth corrections is found in Figure 13. Arrows show the migration from the initial literature value. In the y- axis the arrow points downwards if the population density around the earthquake site is higher compared to Haute-Sorne (e.g. Basel) and upwards if the population density is lower (e.g. Vaz). In the x-Axis the magnitude correction is negative (arrow points to the left) if the hypocenter of an earthquake was deeper than 5 km (e.g. Waldkirch). This means, that if the earthquake would have been shallower, less energy/moment/ M_w would have been needed to cause an equal amount of damage. The correction is positive (arrow points to the right, e.g. Neunkirchen) if the hypocenter was shallower than 5 km, meaning a deeper event would need more energy release to cause an equal damage compared to a shallow one.

VERTRAULICH

B. EMS 98 Intensity scale

The EMS 98 intensity scale was added to better illustrate intensities, shown in Figure 6

EMS-98 Intensity	Felt	Impact	Magnitude (Approximat Value)	Building Damage (Masonry)
I	Not felt	Not felt	2	
II-III	Weak	Felt indoors by a few people. People at rest feel a swaying or light trembling.	3	
IV	Light	Felt indoors by many people, outdoors by very few. A few people are awakened. Windows, doors and dishes rattle.	4	
V	Moderate	Felt indoors by most, outdoors by few. Many sleeping people wake up. A few are frightened. Buildings tremble throughout. Hanging objects swing considerably. Small objects are shifted. Doors and windows swing open or shut.	5	
VI	Strong	Many people are frightened and run outdoors. Some objects fall. Many houses suffer slight non-structural damage like hair-line cracks and falling of small pieces of plaster.	6	
VII	Very strong	Most people are frightened and run outdoors. Furniture is shifted and objects fall from shelves in large numbers. Many well-built ordinary buildings suffer moderate damage: small cracks in walls, fall of plaster, parts of chimneys fall down; older buildings may show large cracks in walls and failure of in-fill walls.	7	
VIII	Severe	Many people find it difficult to stand. Many houses have large cracks in walls. A few well built ordinary buildings show serious failure of walls, while weak older structures may collapse.	8	
IX	Violent	General panic. Many weak constructions collapse. Even well built ordinary buildings show very heavy damage: serious failure of walls and partial structural failure.	9	
X+	Extreme	Most ordinary well built buildings collapse, even some with good earthquake resistant design are destroyed.	10	

© Swiss Seismological Service

Figure 14: EMS 98 Intensity scale, information taken from SED website.

C. Explanation of exceedance probability and rate of occurrence

A short appendix is added to explain the difference between exceedance probability and cumulative rate of occurrence.

In seismology, seismic hazard is usually expressed in terms of exceedance probability. For example a standard seismic hazard map shows a 10% exceedance of ground motion levels within a time span of 50 years. In this study exceedance probability is calculated as follows,

$$Pr_{exceed} = 1 - e^{-N_{cum}}$$

where N_{cum} is the cumulative number of earthquakes greater or equal than a given magnitude. N_{cum} is taken from the risk studies handed in to the Canton (scientific reports E4¹⁰ & E5¹¹). No specific time interval was chosen, instead the risk of the entire stimulation was presented.

The OPAM uses a different terminology in expressing risk. Here risk is given as 'yearly probability' which is an annual cumulative rate of occurrence. To be consistent with the OPAM risk axis, the seismic exceedance probability needs to be converted to annual-cumulative rate of occurrence:

$$N_{cum} = (-\ln(1 - Pr_{exceed}))$$

For the stimulation process the one year time interval of OPAM is too long, as the stimulation process will be shorter (approx. half a year). For a conservative OPAM-type estimate of risk (Figure 15), it is assumed that the stimulation last exactly one year, however one could scale down risk with the ratio of stimulation time vs. one year. To illustrate the difference in risk measures, Figure 15 shows both measures of risk, exceedance probability and yearly cumulative rate of occurrence in one plot.

Note however, that regardless of the representation of risk, the loss-axis remains unchanged. Losses always remain below the threshold of 64¹² Mio CHF where OPAM starts to apply.

¹⁰ Q-con GmbH: Bewertung des seismischen Risikos durch ein EGS Projekt in der Gemeinde Haute-Sorne; Hauptuntersuchung

¹¹ Geo-Energie Suisse AG: Probabilistic seismic hazard analysis of a geothermal project in the Haute-Sorne community

¹² inflation and building index corrected value, initially 50 Mio CHF based on building values of 1996

VERTRAULICH

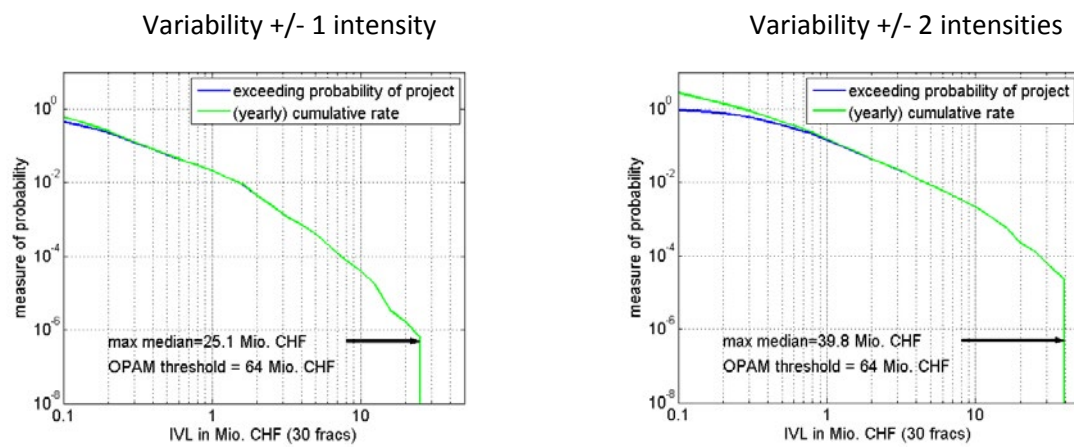


Figure 15: Comparison between exceedance probability and cumulative occurrence rate. Regardless of the measure of probability, physical constraints stop losses at levels before OPAM applies.

VERTRAULICH

D. Injuries

Method

The estimation of injured people after an earthquake is similar to the assessment of casualties described in Chapter 5.1 (see also Landtwing, 2012 for a detailed description). The number of injured persons is based on loss estimation models of QLARM (Earthquake Loss Assessment for Response and Mitigation), Trendafiloski et al., 2011 and STEER (short- Term Earthquake Risk Assessment), van Stiphout, 2009. Both QLARM and STEER use five different damage grades according to HAZUS (1999). Injury matrices derived from HAZUS are then used to transfer damage information obtained by the deterministic models in Chapter 2 to the number of injured persons. Note that injury matrices of HAZUS differentiate between slight, moderate and serious injuries. For simplicity these three classes are combined into one single class 'injuries'. The corresponding logic tree is shown in Figure 16. Compared to financial loss calculations, the number of branches is reduced, because only one injury function is used.

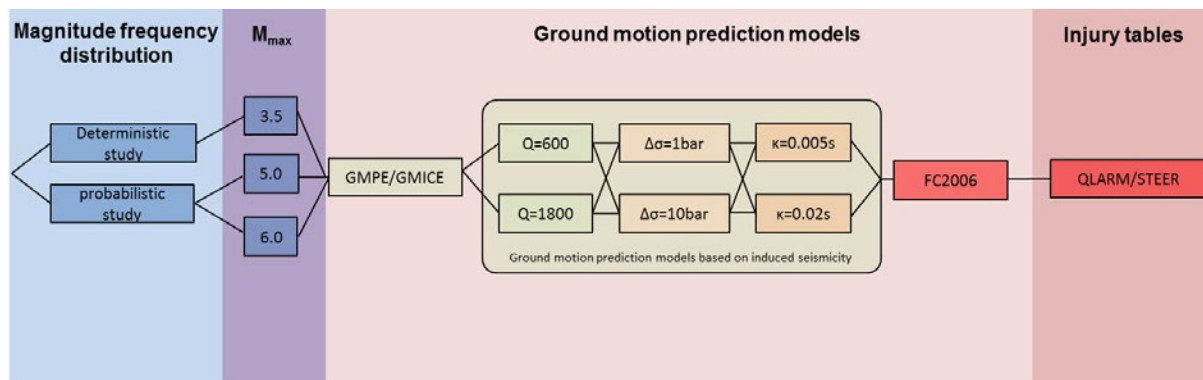


Figure 16: logic tree to calculate injuries. In analogy to Figure 9 and Figure 10 different weighting schemes can be applied.

Results

The number of injuries is plotted against magnitude in Figure 17. For comparison literature data of injuries, adapted to the population density of Haute-Sorne (see Appendix A) is plotted on top. All injury data, where corresponding building code information is assumed to comply with Swiss standards, fall within the 1σ boundaries. For completeness reasons (listed in Table 7) injury data of the Emilia Romagna aftershock and the Lorca earthquake in 2011 are also shown. Both cases are special and are not suited for a comparison to Haute-Sorne conditions. Concerning the 2011 Lorca earthquake, experts blamed poor building design for the high number of injuries and casualties. The damaged buildings, which lead to a high number of injuries (multi-floor buildings with concrete frames and brick fillings) are not representative for buildings in Haute-Sorne and Swiss building standards. Concerning the Emilia Romagna aftershock, further damage to already damaged buildings lead to a high number of injuries, therefore building stock information is also not representative to

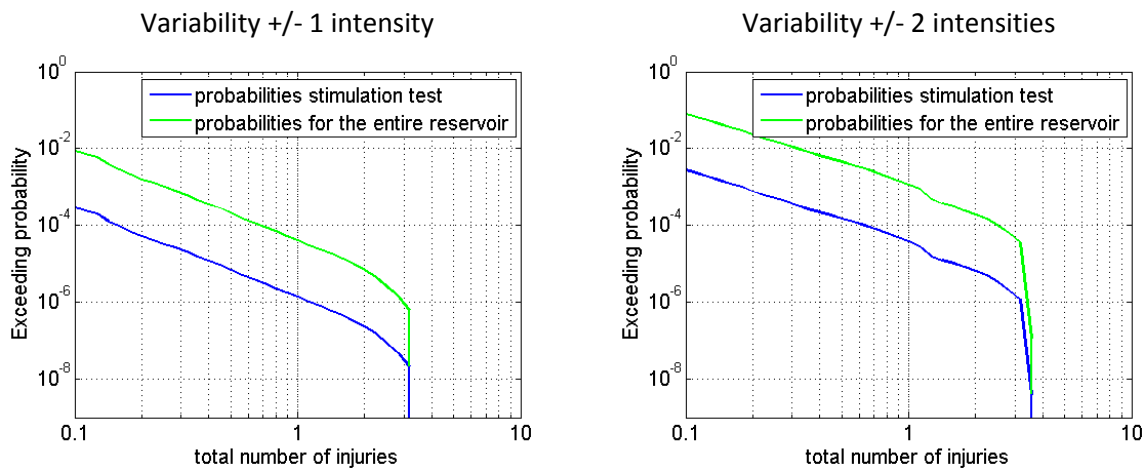


Figure 18: Exceeding probabilities of injured persons for a variability of ± 1 intensity (left) and ± 2 intensity units (right).

E. Additional plots including all branches

This chapter contains additional plots, showing all curves of the logic tree for all mentioned weightings and variabilities of previous chapters. Note that the individual branches (in black) remain identical regardless of weighting; however, the best estimate of maximum insured value loss or injuries (colored curves) changes accordingly. Essential information regarding best estimates of maximum insured value loss is summarized in Table 4 & Table 5.

Intensity plots with a linear probability axis (Figure 6) for different weighting schemes look identical. Changes in exceedance probability are only visible at low probabilities Therefore intensity plots are plotted in log scale.

Intensities (equal weighting of branches, Mmax: 33%/33%/33% -> Figure 9)

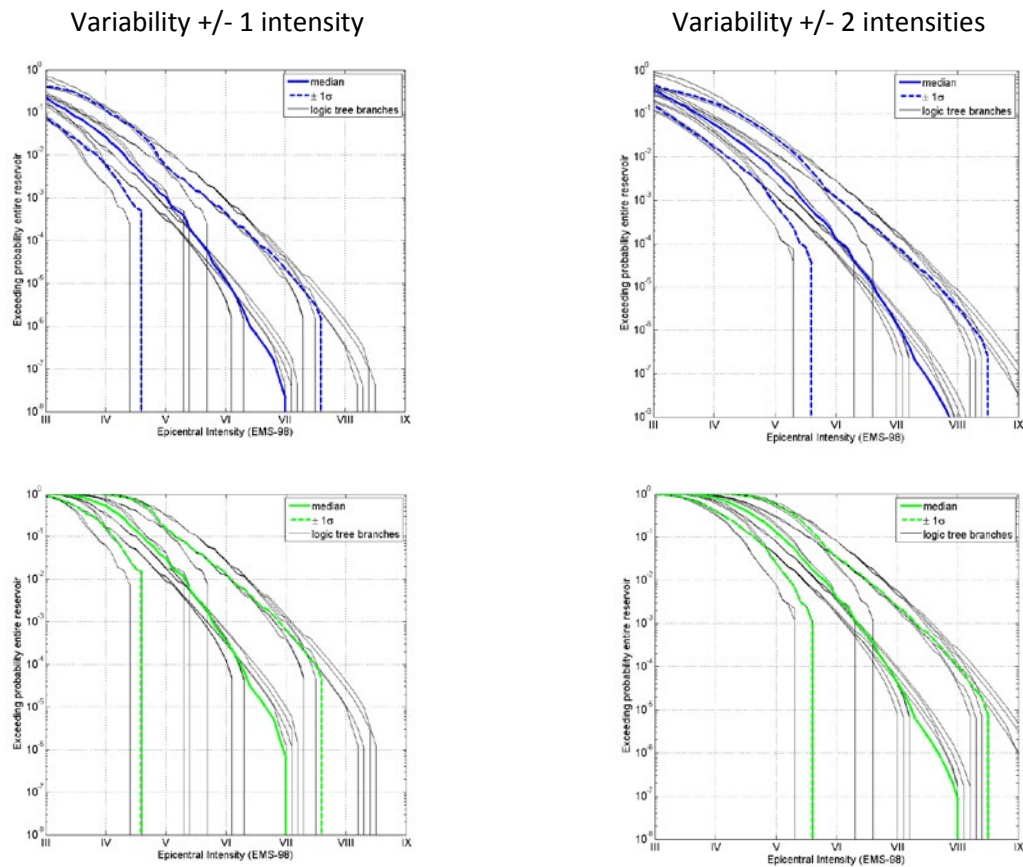


Figure 19: Exceeding probability of intensities for an equal weighting of logic tree branches. Stimulation test in blue, stimulation of the entire reservoir in green.

VERTRAULICH

Intensities (equal weighting of risk studies, weighting Mmax: 50%/25%/25% -> Figure 10):

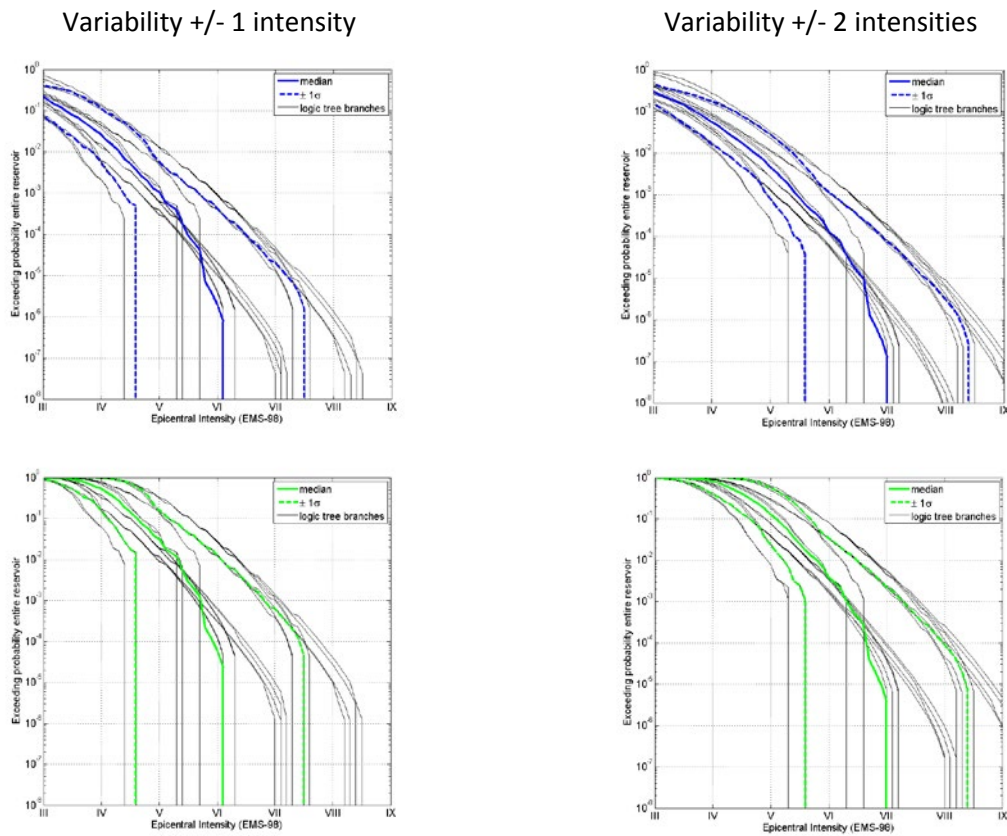


Figure 20: Exceeding probability of intensities for an equal treatment of risk studies. Stimulation test in blue, stimulation of the entire reservoir in green.

Insured value loss (equal weighting of branches, Mmax: 33%/33%/33% -> Figure 9):

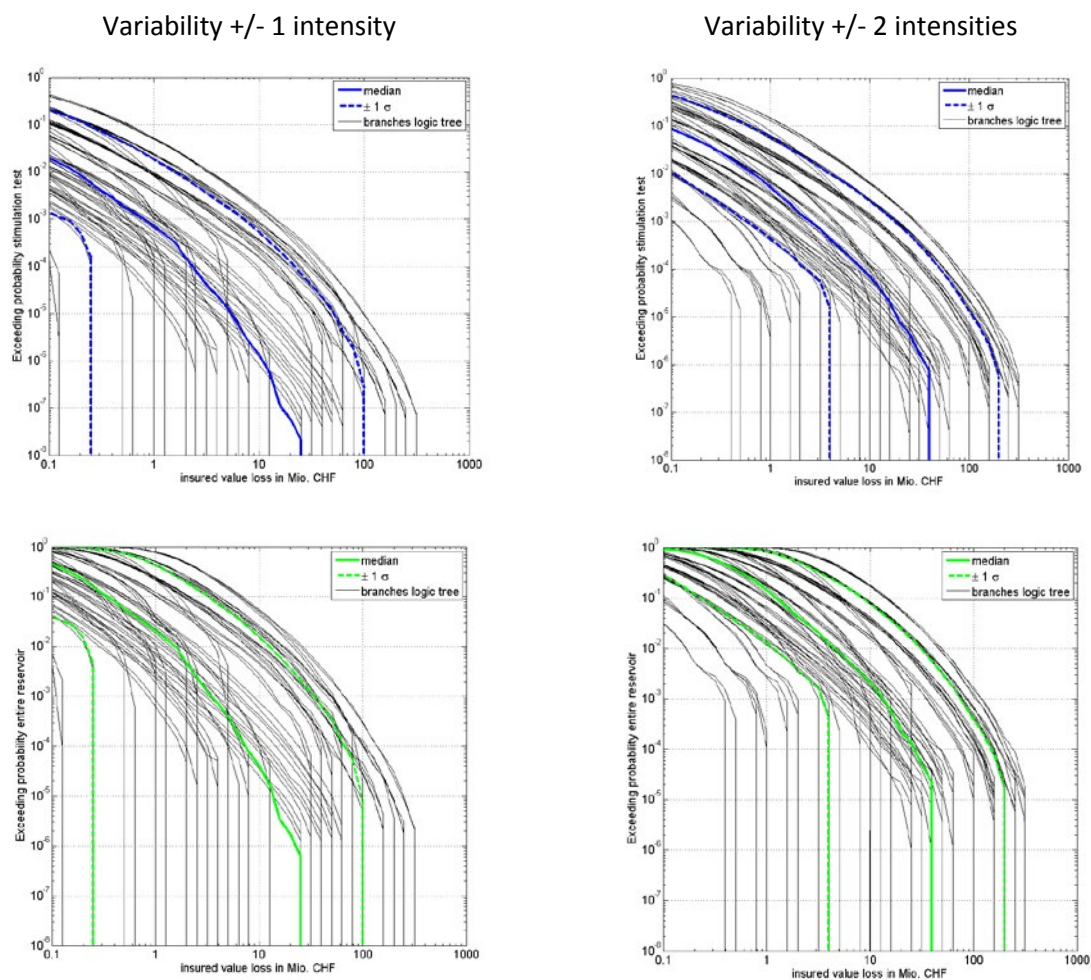


Figure 21: Exceeding probability of insured value loss for an equal weighting of logic tree branches. Stimulation test in blue, stimulation of the entire reservoir in green.

VERTRAULICH

Insured value loss (equal weighting of risk studies, weighting Mmax: 50%/25%/25% -> Figure 10)

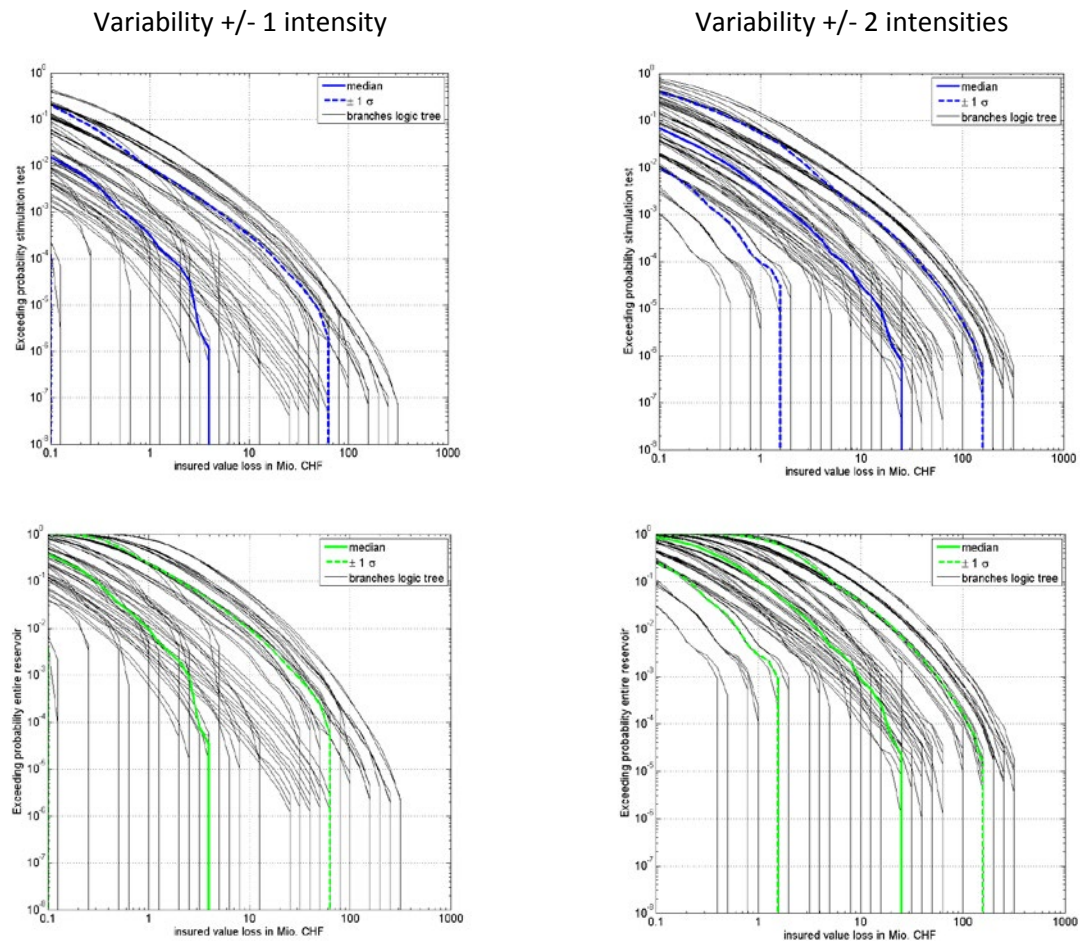


Figure 22: Exceeding probability of insured value loss for an equal treatment of risk studies. Stimulation test in blue, stimulation of the entire reservoir in green.

Injuries (equal weighting of branches, Mmax: 33%/33%/33% -> Figure 9)

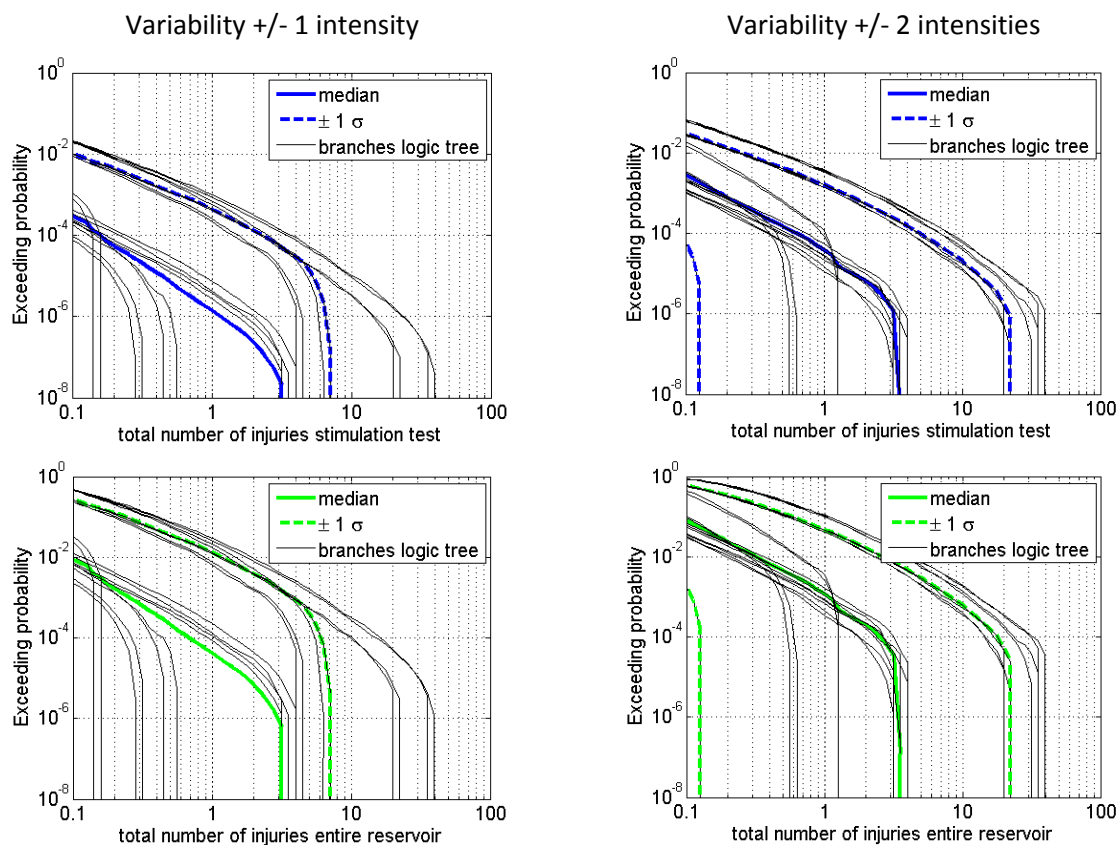


Figure 23: Exceeding probability of injuries for an equal weighting of logic tree branches. Stimulation test in blue, stimulation of the entire reservoir in green.

Injuries (equal weighting of risk studies, weighting Mmax: 50%/25%/25% -> Figure 10)

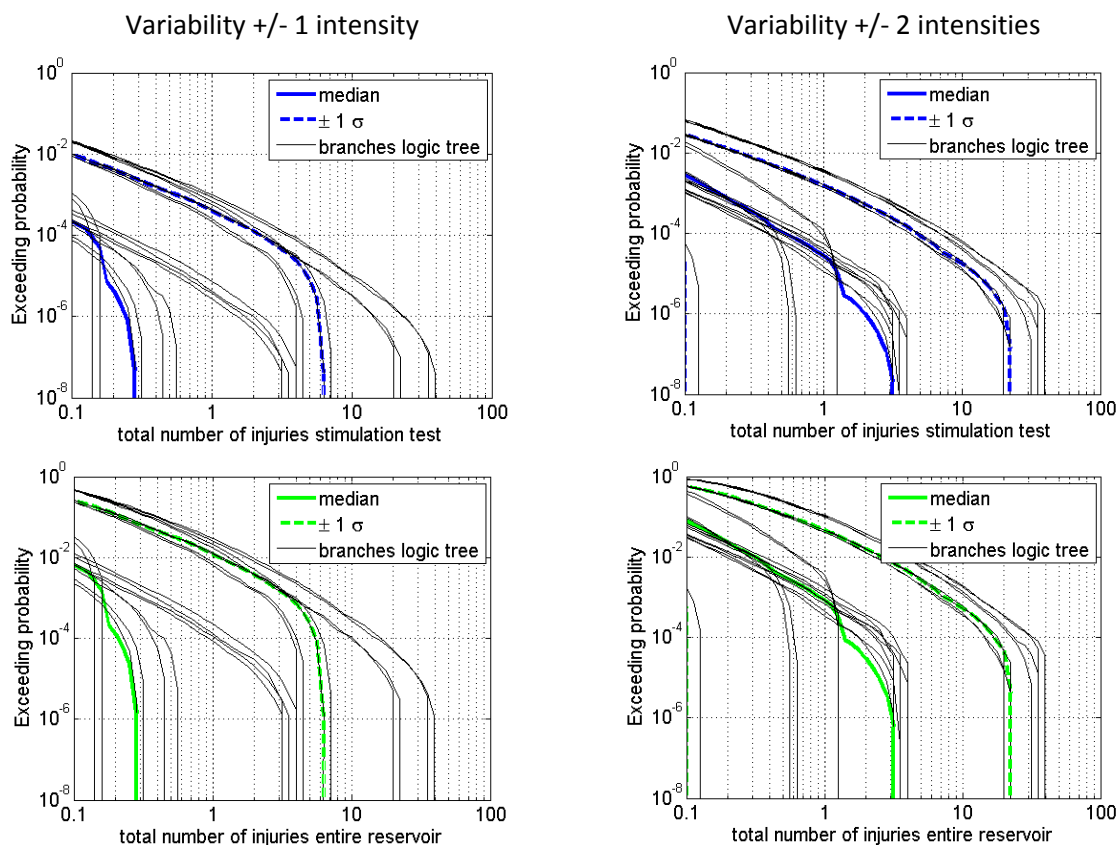
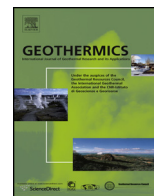


Figure 24: Exceeding probability of injuries for an equal treatment of risk studies. Stimulation test in blue, stimulation of the entire reservoir in green.

F. Geothermics paper, Mignan et al., 2015



Induced seismicity risk analysis of the 2006 Basel, Switzerland, Enhanced Geothermal System project: Influence of uncertainties on risk mitigation



A. Mignan*, D. Landtwing, P. Kästli, B. Mena, S. Wiemer

Swiss Seismological Service, ETH Zürich, Sonneggstrasse 5, 8092 Zürich, Switzerland

ARTICLE INFO

Article history:

Received 24 March 2013

Accepted 16 May 2014

Keywords:

Enhanced Geothermal System

Basel

Risk analysis

Uncertainty

Risk mitigation

ABSTRACT

We present a probabilistic seismic risk analysis of the 2006 Basel Enhanced Geothermal System (EGS) experiment. We combine induced seismicity time-dependent hazard with the RISK-UE macroseismic method and propose a logic tree approach to capture epistemic uncertainties. We find that the expected losses vary over several orders of magnitude for the tested parameters. It indicates that the previous Basel EGS seismic risk study (SERIANEX), which did not include epistemic uncertainties, led to subjective estimates. We address the issue of decision-making under uncertainty by discussing the role of model ambiguity in a simple traffic light system for EGS seismic risk mitigation.

© 2014 Elsevier Ltd. All rights reserved.

1. Introduction

The Deep Heat Mining Project (Häring et al., 2008) to exploit the geothermal potential of the crystalline rocks below the city of Basel, Switzerland, was abandoned in 2009 due to unacceptable risk associated to increased seismic activity during and following hydraulic stimulation (Baisch et al., 2009). The largest induced earthquake ($m_L = 3.4$; $M_w = 3.2$, 8 December 2006) was widely felt by the local population and provoked slight non-structural damage to buildings, estimated to several millions Swiss Francs (CHF) (e.g., Baisch et al., 2009; Giardini, 2009; Kraft et al., 2009). Baisch et al. (2009) (hereafter also referred to as SERIANEX study – a non peer-reviewed report) concluded that “the Basel site might not be favourable for developing an Enhanced Geothermal System (EGS)” due to a high population density and high tectonic activity rate. A high density of population is however sought after since it is more profitable if customers are close to the energy source (for heating, in addition to electricity production).

The purpose of an EGS is to produce geothermal energy on a commercial scale in environments where the connection from the well to the reservoir, or the hydraulic conductivity of the

reservoir itself, is limited. It thus requires to enhance the productivity of the existing reservoir, i.e. the connected network of cracks through which fluids can circulate. This is achieved by injecting fluid under high-pressure into a borehole (e.g., Smith, 1983; Brown et al., 2012). Although considered as an attractive environment-friendly energy source, applications are currently limited due to induced seismicity (e.g., Majer et al., 2007; Giardini, 2009). The termination of the Basel EGS project is one of the best examples of the issues faced with induced seismicity. We should also mention the case of the EGS project of Soultz-sous-Forêts, France (e.g., Charléty et al., 2007), where earthquakes of magnitude $M < 3$ prompted concerns by the local population. No structural damage was caused by these events but a number of residents did put in claims to insurance companies, which were turned down after close examination (Majer et al., 2007).

As noted by Bommer et al. (2006), innovative risk reduction strategies are possible in the scope of induced seismicity since one can manage the risk through control of the hazard, in contrast with standard seismic risk mitigation where only an intervention on vulnerability and/or exposure is feasible. Traffic-light systems have been proposed to determine when the risk associated to induced seismicity reaches an unacceptable level and thus when the EGS operations must be modified or stopped (e.g., Bommer et al., 2006; Häring et al., 2008; Giardini, 2009; Convertito et al., 2012). However, we see three main issues, which may hamper the application of a traffic-light system: (1) the “induced seismicity hazard mitigation paradox”, which is that the largest induced event commonly

* Corresponding author at: Swiss Seismological Service, ETH NO H66, Sonneggstrasse 5, CH-8092 Zurich, Switzerland. Tel.: +41 044 633 71 46; fax: +41 044 633 10 65.

E-mail address: arnaud.mignan@sed.ethz.ch (A. Mignan).

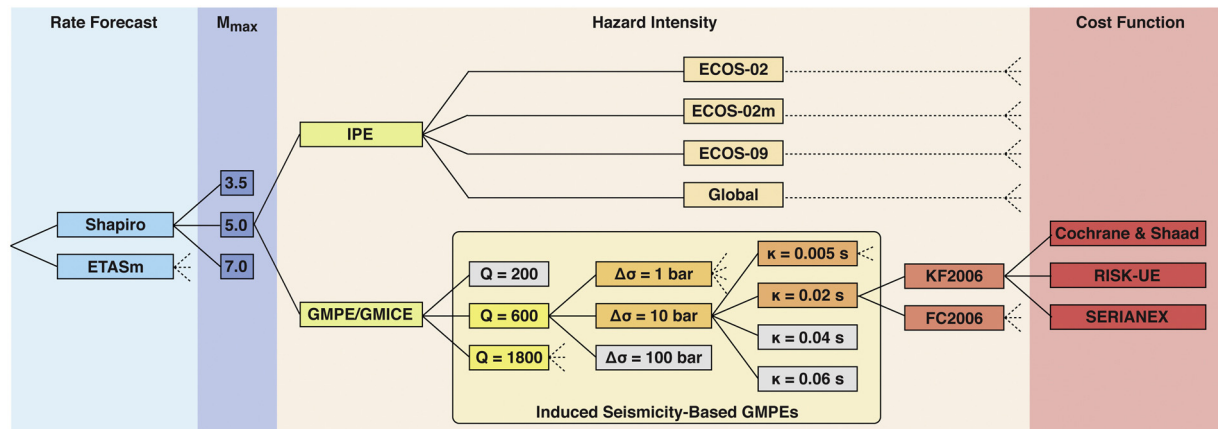


Fig. 1. Logic tree representing the different input parameters and models tested. The components of the logic tree are described in detail in Section 2. All paths have equal weights except for the GMPE parameters represented in grey, for which a null weight is fixed based on parameter estimations in Switzerland.

occurs after shut-in (e.g., Majer et al., 2007; Baisch et al., 2010). The hazard increase after shut-in can be explained by a change in the b -value, which origin remains to be understood (Barth et al., 2013); (2) biased decision threshold due to some ambiguity on hazard and risk estimates and (3) unexpected operational problems. In the present study, we focus on the second issue, which relates to risk mitigation under uncertainty. Uncertainty assessment is particularly challenging for EGS related induced seismicity, where less than 20 relevant case studies exist to date (Evans et al., 2012).

The aim of the present study is twofold: (1) to provide a seismic risk analysis of the 2006 Basel EGS experiment, including model uncertainty, and (2) to illustrate the implications of risk ambiguity for risk mitigation in a simplified traffic-light system. The proposed approach combines time-dependent induced seismicity hazard assessment (Bachmann et al., 2011; Mena et al., 2013) with the RISK-UE macroseismic approach to damage assessment (Lagomarsino and Giovanazzi, 2006; Baisch et al., 2009). Epistemic uncertainties are systematically captured following a logic tree approach, as used in standard PSHA (Kulkarni et al., 1984) and results compared to the SERIANEX study in which model uncertainties were not considered. To our knowledge, the present study is the first one to consider uncertainties in a systematic way for EGS seismic risk analysis. Results apply to other technologies involving fluid injection into the subsurface, as for example wastewater disposal (e.g., Horton, 2012), carbon capture and sequestration (e.g., Stirling et al., 2012; Zoback and Gorelick, 2012), secondary recovery of oil and gas (water flooding) and the exploitation of unconventional gas reservoirs (shale gas, hydraulic fracturing) (National Research Council, 2012). It is important to state that the analysis presented in the present article should not be considered as a definitive seismic loss assessment of the 2006 Basel EGS project. Use of other models or other methods may yield different outcomes. Results are presented only to illustrate the influence of uncertainties on risk mitigation.

2. Input models

We first present the different input models and related data used in the present study, most of which can be represented in a logic tree structure. Fig. 1 shows the logic tree proposed for the Basel EGS risk analysis, which would also apply to other EGS sites in Switzerland. Other models and model parameters may be required in other tectonic settings. The different levels of the logic tree are described below.

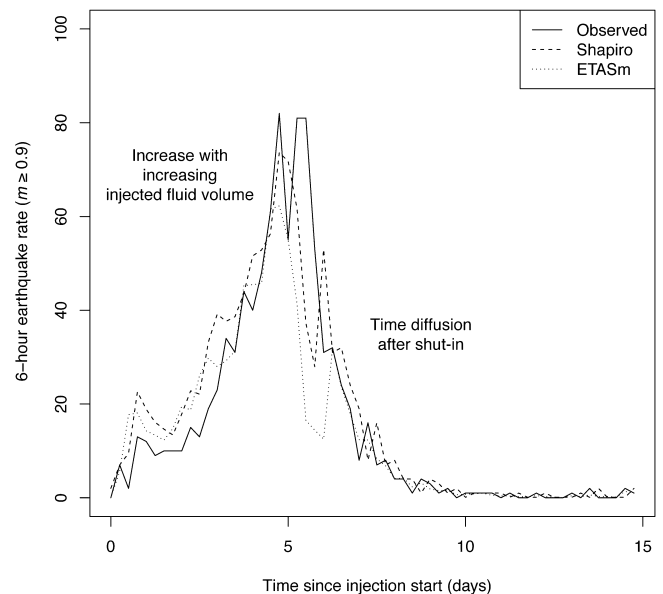


Fig. 2. Basel induced seismicity 6-h rate time series, observed and forecasted. The observed rates and Shapiro and ETAS forecasts are taken from Mena et al. (2013).

2.1. Hazard rate

The probability of occurrence of induced earthquakes is determined from induced seismicity forecast models. We tested the results of two models (Shapiro SR and ETAS E5) computed by Mena et al. (2013), which are based on a 6-h pseudo-prospective approach (Fig. 2). Both models are based on the well-established correlation between induced seismicity activity and fluid injection (Majer et al., 2007 and references therein).

The Shapiro model (e.g., Shapiro et al., 2007; Shapiro and Dinske, 2009; Shapiro et al., 2010) suggests that (1) the number of induced earthquakes increases approximately proportionally to the injected fluid volume and that (2) the diffusion of induced seismicity with time in the post-injection phase can be described by the modified Omori law (Langenbruch and Shapiro, 2010). The original ETAS (Epidemic-Type Aftershock Sequence) model (Ogata, 1988) considers stationary background seismicity and aftershock diffusion based on the modified Omori law. Here, each event (regardless of being a background event or an aftershock) can produce aftershocks. To make the ETAS model applicable to induced seismicity,

Table 1

Intensity Prediction Equations (IPEs) for shallow/near-range events and Ground Motion to Intensity Conversion Equations (GMICEs) including small intensities. Intensities I are expressed in the EMS-98 scale except for the global IPE in which no specific Cancani scale is used and the FC GMICE in which the MCS scale is used. Peak Ground Velocity (PGV) is expressed in m/s. Magnitudes are expressed in moment magnitude M_w .

Name	Equation	Reference
Intensity Prediction Equations (IPEs)		
ECOS-02	$I = 1.27 M_w - 0.043 d_e + 0.096$	Fäh et al. (2003)
ECOS-02m	$I = 1.5248 M_w - 0.043 d_e - 0.9079$	Alvarez-Rubio et al. (2012)
ECOS-09	$I = \frac{M_w - c_2 \ln\left(\frac{d_h}{30}\right) - c_3(d_h - 30) - c_0}{c_1}$ with $c_0 = \beta$, $c_1 = \alpha$, $c_2 = -\alpha a$ and $c_3 = -\alpha b$; $a = -0.69182$, $b = 0.00084$, $\alpha = 0.7317$ and $\beta = 1.2567$.	Fäh et al. (2011)
Global	$I = c_0 + c_1 M_w + c_2 \ln \sqrt{d_h^2 + (m_1 + m_2 \exp(M_w - 5))^2}$ with $c_0 = 2.085$, $c_1 = 1.428$, $c_2 = -1.402$, $m_1 = -0.209$ and $m_2 = 2.042$.	Allen et al. (2012)
Ground Motion-Intensity Conversion Equations (GMICE)		
FC2006	$I = 1.80 \log(PGV) + 8.69$; $\sigma = 0.71$	Facciolo and Cauzzi (2006)
KF2006	$I = (\log(PGV) + 4.1962)/0.4418$; $\sigma = 1.22$	Kästli and Fäh (2006)

Bachmann et al. (2011) defined a non-stationary background rate based on an approach similar to the Shapiro model, by relating the background rate to the volume injected. We hereafter refer to this modified version of ETAS by the term ETASm.

While many other models exist (see review by Goertz-Allmann and Wiemer, 2013), we only considered the two statistical forecast models, which we believe represent the main aspects of the process during and after injection and which have been shown to yield a good fit to the Basel data (Fig. 2; Mena et al., 2013). Information about hydraulic stimulation during the Basel EGS project is summarized in Häring et al. (2008) and information about the characteristics of the Basel induced earthquakes can be found in Mukuhira et al. (2013) and references therein.

2.2. Hazard intensity

We considered both Intensity Prediction Equations (IPEs) and Ground Motion Prediction Equations (GMPEs) for hazard assessment. We first determined seismic hazard intensity by using IPEs with intensity I defined in the European Macroseismic Scale (EMS-98; Grünthal, 1998). Using a macroseismic intensity scale facilitates communicating shaking levels in terms of nuisance to the population and damage. It is used in the present study to be consistent with the SERIANEX approach in which damage assessment is based on the RISK-UE macroseismic method (Lagomarsino and Giovinazzi, 2006) (see Section 3). We tested four macroseismic Intensity Prediction Equations (IPEs), three based on the Earthquake Catalogue Of Switzerland (ECOS), ECOS-02 (Fäh et al., 2003), ECOS-02 m (Alvarez-Rubio et al., 2012) and ECOS-09 (Fäh et al., 2011) and one based on global data (Allen et al., 2012). In all cases, we used the relationships defined for short distances (<50–70 km) and for shallow events (depth < 20 km). Equations are given in Table 1. IPEs for Switzerland are expressed in the EMS-98 scale. Allen et al. (2012) assumed equivalency between different 12-degree intensity scales (so-called Cancani scales) since they are broadly compatible with one another (Musson et al., 2010). We followed the same logic by assuming that the intensities obtained in the global model are equivalent to the ones of the EMS-98 scale. Allen et al. (2012) also considered aleatory uncertainty, which is approximated by the distance dependent function:

$$\sigma = s_1 + \frac{s_2}{1 + (d_{\text{hyp}}/s_3)^2} \quad (1)$$

with σ the standard deviation (commonly called sigma), $s_1 = 0.82$, $s_2 = 0.37$ and $s_3 = 22.9$. Allen et al. (2012) showed that inclusion of site correction factors results in almost no improvement in median residuals. We assumed, as recommended by Allen et al. (2012), that site amplification variability is included in the sigma of Eq. (1). For the three other IPEs, we fixed $\sigma = 1$, which is close to the results of

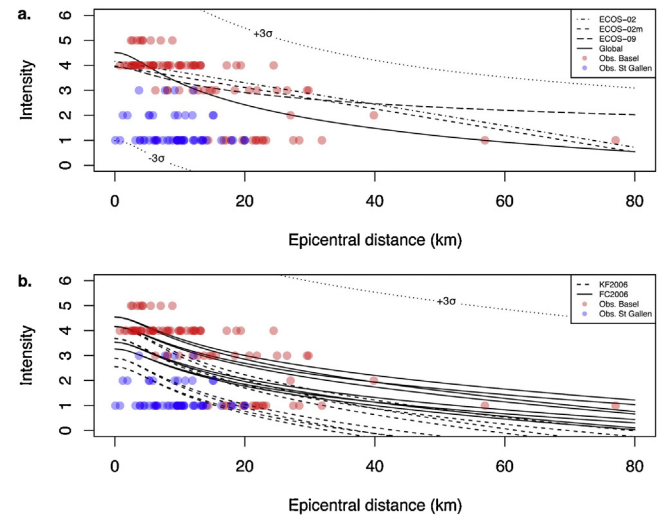


Fig. 3. Intensity as a function of epicentral distance for an earthquake of moment magnitude $M_w = 3.2$ and 4.6 km deep. (a) Intensity Prediction Equations (IPEs). Dotted curves represent the 3-sigma bounds of the global IPE model. (b) Ground Motion to Intensity Conversion Equations (GMICEs). Dotted curves correspond to the 3-sigma bounds of the 2 extreme models. Points represent the observed intensities for the $M_w = 3.2$ Basel event and the $M_w = 3.3$ St. Gallen event that occurred at 4.7 and 4.5 km deep, respectively.

Eq. (1) for $d_{\text{hyp}} < 15$ km. A same choice was made in the SERIANEX study for the ECOS-02 model. Fig. 3a shows the macroseismic intensity as a function of epicentral distance predicted by the different IPEs and a comparison with the intensities felt during the largest events that occurred during the 2006 Basel sequence (Ripperger et al., 2009) and the 2013 St. Gallen sequence (data from the Swiss Seismological Service – magnitude $m_L = 3.5$; $M_w = 3.3$). It shows that the observed intensities for induced seismicity in Switzerland fall within the 3-sigma bounds of the four proposed IPEs.

More sophisticated damage evaluation approaches exist, based on instrumental parameters (e.g., Crowley et al., 2004; Lagomarsino and Giovinazzi, 2006). Those are not tested here due to exposure data limitations. However we considered GMPEs by translating Peak Ground Velocity (PGV) values into expected intensities by using Ground Motion to Intensity Conversion Equations (GMICEs). We considered the 36 stochastic GMPEs defined specifically for induced seismicity by Douglas et al. (2013) and (2) GMICEs defined for relatively small intensities (Facciolo and Cauzzi, 2006; Kästli and Fäh, 2006). The GMPEs are available as supplementary material in Douglas et al. (2013) while the GMICEs are given in Table 1. To avoid any systematic bias due to the fact that instrumental measures are obtained on hard-rock sites, we corrected GMICE estimates by adding the amplification of felt intensities, assumed to

Table 2
Cost functions relating damage grade (DG) to mean damage ratio (MDR). From [Cochrane and Shaad \(1992\)](#); RISK-UE (given in [Baisch et al., 2009](#)) and SERIANEX study ([Baisch et al., 2009](#)).

DG	Damage description	Damage state	MDR Cochrane and Shaad	MDR RISK-UE	MDR SERIANEX
0	No damage	None	0%	0%	0%
1	Negligible to slight damage	Minor	5%	1%	2%
2	Slight structural and moderate non structural	Moderate	20%	10%	15%
3	Moderate structural and heavy non-structural	Severe	58%	35%	55%
4	Heavy structural and very heavy non-structural	Very heavy	94%	75%	91%
5	Very heavy structural and partial or total collapse	Destruction	100%	100%	100%

be 0.47, based on the work of [Fäh et al. \(2010\)](#) (see also [Edwards and Fäh, 2013](#)). Also, as recommended by [Douglas et al. \(2013\)](#), we selected only 8 GMPEs out of the original 36 stochastic models in order to reduce epistemic uncertainties. For Switzerland, [Edwards and Fäh \(2013\)](#) suggested $Q = 1200$ (crustal attenuation model) and $\kappa = 0.016$ s (hard-rock site specific attenuation). Moreover, stress drops measured for the largest Basel and St Gallen earthquakes were respectively $\Delta\sigma = 10$ bar and 3 bar (pers. comm., Benjamin Edwards, 2013). We affixed a null weight for parameters outside of these ranges, as shown in [Fig. 1](#). The impact of using a selection of 8 GMPEs instead of the original 36 GMPE models is evaluated in [Section 4.1](#).

In the case of intensities converted from ground motion, aleatory uncertainty is defined by

$$\sigma = \sqrt{\sigma_{\text{GMPE}}^2 + \sigma_{\text{GMICE}}^2} \quad (2)$$

with

$$\sigma_{\text{GMPE}} = \sqrt{\phi_{\text{ss}}^2 + \tau_{\text{Basel}}^2} \quad (3)$$

in which $\phi_{\text{ss}} = 0.535$ is the within-event variability and $\tau_{\text{Basel}} = 0.558$ the between-event variability defined in the natural log space of the PGV ([Douglas et al., 2013](#)). σ_{GMICE} is given in [Table 1](#). After conversion of σ_{GMPE} into intensity, we obtained $\sigma_{\text{GMPE}+\text{FC2006}} = 0.93$ and $\sigma_{\text{GMPE}+\text{KF2006}} = 1.44$ (following Eq. (2)). [Fig. 3b](#) shows that intensities as a function of distance derived from GMICES are consistent with observed intensities and with IPE results.

2.3. Other hazard parameters (*b*-value and M_{max})

The *b*-value of the Gutenberg Richter law ([Gutenberg and Richter, 1944](#)) is fixed to $b = 1.58$ for the injection period and to $b = 1.15$ for the post-injection period based on the analysis made by [Bachmann et al. \(2011\)](#) for the 2006 Basel induced seismicity sequence. The α -value is calculated from *b* and the 6-day forecasted rates ([Fig. 2](#)).

We tested $M_{\text{max}} = 3.7$, 5.0 and 7.0 (e.g., [Mena et al., 2013](#)). $M_{\text{max}} = 3.7$ is constrained by the size of the reservoir ([Baisch et al., 2009](#)). When assuming $M_{\text{max}} = 5.0$ or 7.0, we allow events at very small probabilities that are much larger than the volume influenced by high fluid pressures, thus capturing also the possibility that earthquakes are triggered prematurely on larger and unknown faults pre-loaded by tectonic stresses. While in cases where the location and loading state of faults is well known it may be more accurate to consider these faults explicitly, we argue that this is almost never the case. Faults in granitic rocks can hardly be imaged, nor do we have knowledge on their loading state; nor can it be excluded that a rupture, once started, extends significantly beyond the area of high pore pressure. Therefore, extending the forecasted magnitudes to the tectonically derived M_{max} is in our view a conservative approach ([Wiemer et al., 2009](#)). Noteworthy, a magnitude $M_w = 6.6$ earthquake occurred in 1356 in the Basel region (e.g., [Grünthal and Wahlström, 2012](#)). More information on the

tectonics of the Basel region can be found in [Ustaszewski and Schmid \(2007\)](#).

2.4. Basel building stock

We used the Basel building stock published in the SERIANEX report. It comprises 79 settlements (assumed to be points and with Basel subdivided into 19 districts) located within a 14 km radius around the borehole of the Basel EGS. For each settlement, the following information is available: Total number of buildings, number of buildings per building class and total insured value (exposure) for residences only ([Tables A1 and A2](#)). The exposure is then disaggregated to the building level by dividing the total exposure by the total number of buildings. The centre of each settlement has been located using Swiss national maps published by [swisstopo \(2012\)](#) (see [Tables A1 and A2](#)).

We used the building classification of [Baisch et al. \(2009\)](#) ([Table A3](#)), which distinguishes between 16 classes, including 9 classes from the RISK-UE classification (matching 7 EMS-98 classes) and 7 more defined for the Basel area. Vulnerability index values V_0 are defined for each building class, including probable and less probable ranges V_-/V_+ and V_{--}/V_{++} , following the approach of [Lagomarsino and Giovinazzi \(2006\)](#). Vulnerability factors, which additionally consider the number of storeys, building age and other parameters required in mechanical models, were not included in the present work. We however assumed that the mechanical and macroseismic approaches result in equivalent levels of damage ([Lagomarsino and Giovinazzi, 2006](#)). Epistemic uncertainty in mechanical models is discussed at depth by [Crowley et al. \(2005\)](#). The Basel building stock used in the present study is given in the [Appendix A](#) more detailed dataset can be found in [Baisch et al. \(2009\)](#). Hazard intensity (see [Section 2.2](#)) is computed for each settlement for induced earthquakes occurring at the casing shoe of the injection well Basel 1 ($x_{\text{CH}} = 611,810$ m, $y_{\text{CH}} = 270,535$ m, $z = 4740$ m).

2.5. Cost functions

Damage can be measured in economic terms through the mean damage ratio (MDR), defined as the ratio between the repair cost and the asset cost. We tested 3 cost functions, which relate damage grade to MDR. The functions are from [Cochrane and Shaad \(1992\)](#), RISK-UE (not published in the scope of the RISK-UE project (e.g., [Mouroux and Le Brun, 2006](#)) but provided in [Baisch et al., 2009](#)) and [Baisch et al. \(2009\)](#) ([Table 2](#)). The SERIANEX cost function was calibrated to the insurance claims following the 8 December 2006, $M_w = 3.2$, induced event, as discussed later on.

3. Hazard and risk assessment

3.1. Hazard assessment

We converted induced seismicity rates given in [Fig. 2](#) into probabilities of a given ground motion intensity being exceeded using the standard procedures originally introduced by [Cornell](#)

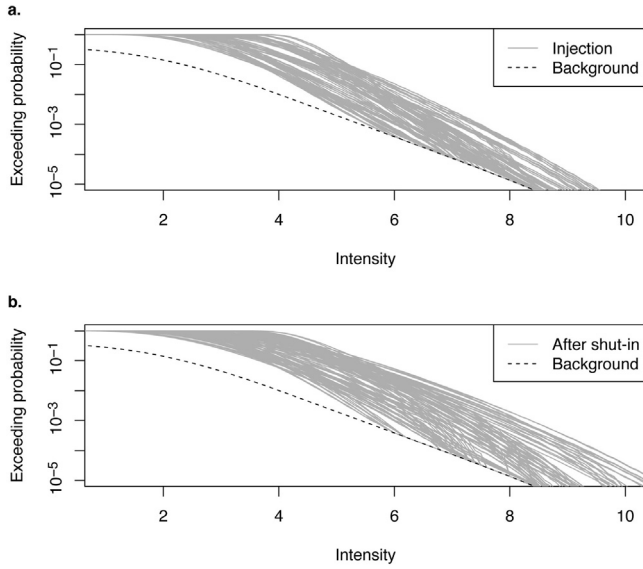


Fig. 4. Seismic hazard curves (including the background hazard) defined by the probability of exceeding a given intensity over a 6-day period for a point located at $d_{hyp} = 10$ km from the borehole. (a) 6-day injection period ($b = 1.58$); (b) first 6 days of the post-injection period ($b = 1.15$). Grey curves correspond to the 120 ($2 \times 3 \times (4 + 8 \times 2)$) different paths of the logic tree, including the background hazard. The dashed curves correspond to background hazard only, defined from $M_{max} = 7.0$ and the ECOS-02 IPE model.

(1968) and Esteva (1970) and more recently applied to short-term aftershock hazard by Wiemer (2001) and Gerstenberger et al. (2005). For a history and review of seismic hazard assessment, see Bommer and Abrahamson (2006) and McGuire (2008).

Fig. 4 shows the seismic hazard curves (including the background hazard) for the 6-day injection period ($b = 1.58$) and for the first 6 days after shut-in ($b = 1.15$) at a distance $d_{hyp} = 10$ km from the borehole. For each period, 120 ($2 \times 3 \times (4 + 8 \times 2)$) curves are shown, representing epistemic uncertainty on rate forecast, M_{max} and hazard intensity (Fig. 1). Our results are not comparable to previous analyses (Bachmann et al., 2011; Mena et al., 2013; Baisch et al., 2009) due in particular to the use of a smaller sigma in Bachmann et al. (2011) and Mena et al. (2013), fixed to 0.5 arbitrarily (pers. comm., Jochen Woessner, 2012), and to the choice made by Baisch et al. (2009) to truncate the normal distribution of macroseismic intensity at 2-sigma while we used 3-sigma. Overall, it means that our results are more conservative than in previous studies (Bommer and Abrahamson, 2006). We also calculated the background hazard curve for a 6-day period with $M_{max} = 7.0$ and the ECOS-02 IPE. The a - and b -values were taken from Wiemer et al. (2009) for seismicogenic zone 15 (Basel, $a = 2.31$, $b = 0.9$). It is represented by the dashed curve in Fig. 4. Results show an important scattering with the probability of exceeding a given macroseismic intensity varying roughly over one to two orders of magnitude.

3.2. Damage assessment

The strategy for damage assessment is identical to the one used by Baisch et al. (2009), which is the RISK-UE macroseismic approach based on classical probability theory and fuzzy-set theory (Lagomarsino and Giovinazzi, 2006). The macroseismic model relates the mean damage grade (MDG or μ_D) to the macroseismic intensity I_{EMS98} and the vulnerability index V_i as follows:

$$\mu_D = 2.5 \left[1 + \tanh \left(\frac{I_{EMS98} + 6.25V_i - 13.1}{Q} \right) \right] \quad (4)$$

with $0 < \mu_D < 5$ and Q the ductility index fixed to $Q = 2.3$ (for representative values). Fig. 5a shows examples of vulnerability curves

based on Eq. (5) for different V_i values. From the MDG, the probability of occurrence of each damage grade (DG) as defined in the EMS-98 scale (Grünthal, 1998) is determined based on a binomial distribution:

$$p_k = \frac{5!}{k!(5-k)!} \left(\frac{\mu_D}{5} \right)^k \left(1 - \frac{\mu_D}{5} \right)^{5-k} \quad (5)$$

with p_k the probability of occurrence of DG_k and $0 \leq k \leq 5$. Damage grades are defined as follows: no damage (DG_0), slight (DG_1), moderate (DG_2), heavy (DG_3), very heavy (DG_4) and destruction (DG_5). Fig. 5b shows the damage grade distribution (DGD) versus intensity for a fixed $V_i = 0.74$, typical of a building of vulnerability class B in the EMS-98 scheme. More details about the macroseismic approach can be found in Lagomarsino and Giovinazzi (2006) and about its application to the Basel EGS project in Baisch et al. (2009). Correspondence between building vulnerability class and vulnerability index is given in Table A3.

3.3. Loss assessment and calibration

The DGD is computed for each building class represented in any given settlement, leading to the number of buildings per DG per building class. This number is then summed over all building classes. Finally, the insured value loss (IVL) per settlement is:

$$IVL = \sum_{k=0}^{k=5} \text{number of buildings } (DG_k) \times MDR(DG_k) \times IV \quad (6)$$

The total IVL for the Basel region is obtained by summing all settlements' IVLs. Based on this approach, Baisch et al. (2009) obtained surprisingly high amounts of repair costs for an induced event of magnitude $M_w = 3.2$. The RISK-UE macroseismic method is indeed ill defined for small magnitude earthquakes, as there is a non-zero probability of producing damage for EMS-98 intensities IV and below (Fig. 4b), although damage of grade 1 (DG_1) is expected for a few buildings only at intensity V (Grünthal, 1998). Baisch et al. (2009) calibrated the vulnerability curves in the low intensity domain of Eq. (4) by introducing a reduction factor for intensities $III \leq I \leq VI-VII$. This factor, corresponding to the square of the linear equation defined over the abscissa interval [3; 6.5] and ordinate interval [0; 1], was multiplied to the vulnerability curve defined in Eq. (4). Their goal was to match the claims associated to the $M_w = 3.2$ event by assuming that all losses were insured. Using the same input parameters as in the SERIANEX study (i.e., ECOS-02 IPE/SERIANEX cost function) and the same calibration, we found a good agreement with their results with $IVL(M_w = 3.2) = 10,378,473$ CHF versus 10,521,479 CHF in the SERIANEX study (good agreement also found for $M_w = 3.7$ and $M_w = 4.1$ scenarios).

Giardini (2009) indicated that the more than USD 9 million damage claims seemed a high loss for such moderate size earthquakes. It was later indicated that the claims following the $M_w = 3.2$ event were exaggerated and that the real value would be closer to 3 million CHF (pers. comm., Geo-Energy Suisse, 2012). Here we decided to recalibrate the vulnerability curves not based on that value, which remains loosely constrained, but by matching the expected DG distribution to the EMS-98 damage description for vulnerability class B. We chose a reduction factor bounded over $IV \leq I \leq VII$, such that no damage is possible for intensities IV and below and such that damage for intensities VII and above remains the same as for standard seismic risk assessment, this limit corresponding roughly to an earthquake of magnitude 5. The calibrated vulnerability curves are shown in Fig. 5a and the updated damage grade distribution in Fig. 5c. Using the same parameters as previously but with the new calibration, we found the median value $IVL(M_w = 3.2) = 19,407$ CHF, i.e. close to no loss, which is considerably less than the 3 million CHF estimate. This would indicate that the loss estimate is still too high

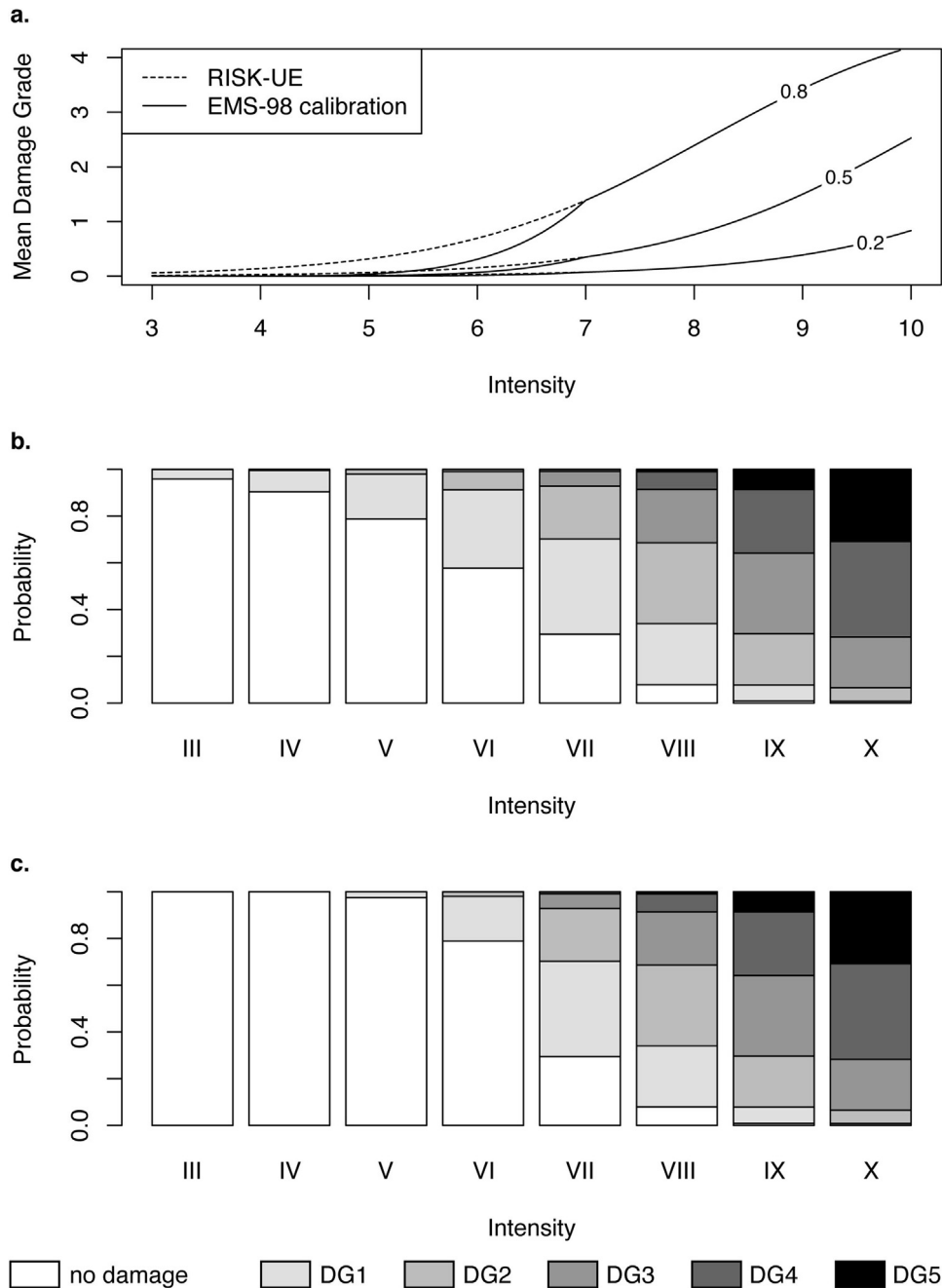


Fig. 5. Damage assessment based on the RISK-UE macroseismic approach (Lagomarsino and Giovinazzi, 2006). (a) Vulnerability curves for different vulnerability index V_i values, determined from Eq. (4) with or without calibration; (b) damage grade distribution for $V_i = 0.74$ (i.e., building of EMS-98 vulnerability class B), determined from Eq. (5). Damage grades at small intensities are inconsistent with the EMS-98 scheme; (c) damage grade distribution after calibration to the EMS-98 scheme.

or that the $M_w = 3.2$ Basel event was somewhat anomalous (severe) or that the SERIANEX model parameters are incorrect.

Fig. 6a shows a series of 60 $((4 + 8 \times 2) \times 3)$ loss curves defined by the total IVL (median value V_0) as a function of earthquake magnitude. Each value on the curve represents one deterministic loss scenario. By including epistemic uncertainty on hazard intensity and cost function (Fig. 1), we obtained $IVL(M_w = 3.2)$ in the range 0 CHF – 4,806,149 CHF. Fig. 6b shows loss curves, which include the role of aleatory uncertainty at the vulnerability level, by considering the less probable vulnerability index V_{++} . In this case, we obtained $IVL(M_w = 3.2)$ in the “less probable” range 0 CHF – 20,477,384 CHF. The estimated 3 million CHF loss remains in the high range of possible values, which would indicate – if correct – that the $M_w = 3.2$ event was indeed severe. We then computed

loss exceedance curves for the 6-day injection period. We generated seismic hazard curves at the 79 settlements and combined the losses expected at each location for each 6-day probability of exceedance (injection phase with $b = 1.58$, V_0 case). Noteworthy, we only took into account the induced seismicity part of the hazard curve to calculate its net impact. Fig. 7a shows a series of 360 $(2 \times 3 \times (4 + 8 \times 2) \times 3)$ loss exceedance curves for a settlement located at 10 km from the borehole. A large scattering of the curves is again obvious with variations over several orders of magnitudes. Finally we computed the 6-day average loss (called the most probable insured value loss (MPIVL) in the SERIANEX study) by integrating the loss exceedance curves and summing the values over all settlements. For comparison with the SERIANEX study, we show the MPIVL distribution for a 12-day injection (twice

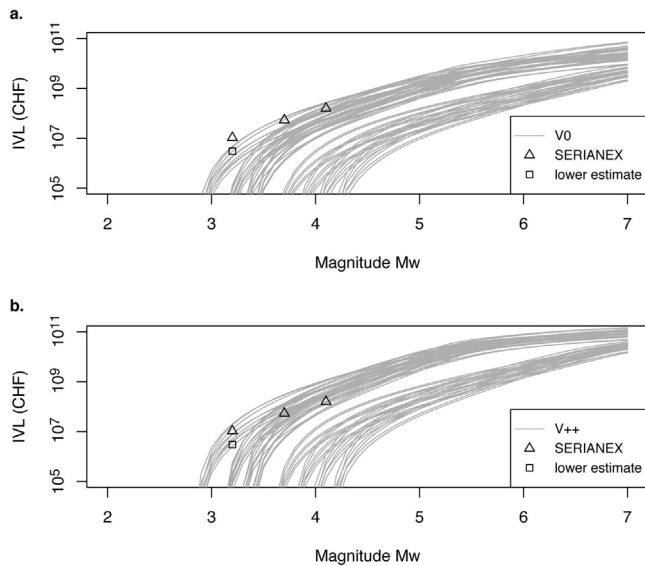


Fig. 6. Loss curves defined by the insured value loss (IVL) as a function of moment magnitude M_w . The 60 $((4+8 \times 2) \times 3)$ curves represent the different paths of the logic tree; (a) median damage based on vulnerability index V_0 ; (b) less probable damage based on vulnerability index V_{++} .

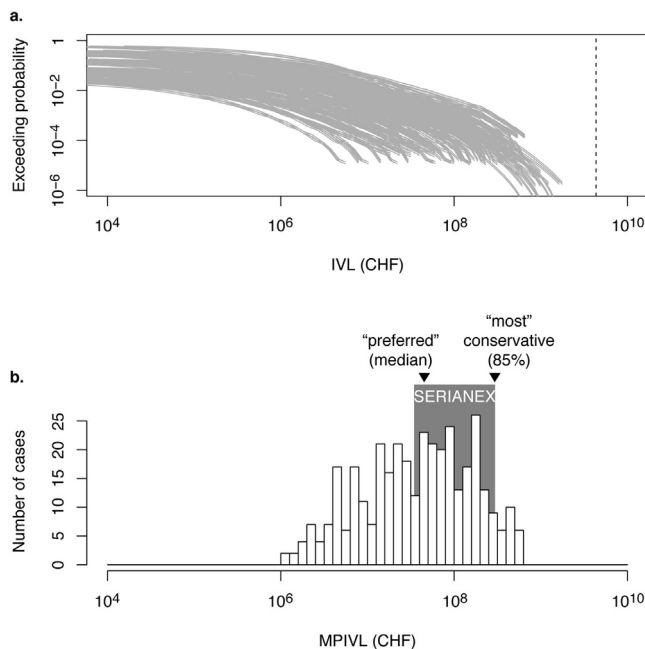


Fig. 7. Probabilistic risk metrics. (a) Probabilistic loss curves defined as the probability of exceeding a given IVL over a 6-day injection period at a settlement located at 10 km from the borehole. The 360 $(2 \times 3 \times (4+8 \times 2) \times 3)$ curves represent the different paths of the logic tree. The vertical line represents the total exposure. (b) Distribution of the most probable insured value loss (MPIVL) over a 12-day injection period (twice the 6-day risk – to be comparable to the SERIANEX study). The grey rectangle represents the range of SERIANEX estimates. Their preferred estimate (45 million CHF) is obtained using the median hazard curve (0-sigma) while their most conservative estimate (300 million CHF) is obtained using the 85% percentile of the hazard curve. In comparison, all of our estimates are based on 3-sigma hazard curves.

the 6-day risk) in Fig. 7b. Crowley and Bommer (2006) and references therein showed that summing over different locations leads to an overestimation of the risk due to an incorrect interpretation of the aleatory variability in the hazard intensity. However we could not make the distinction between intra- and inter-sigma variability for the IPEs and GMICEs considered. We recognize that

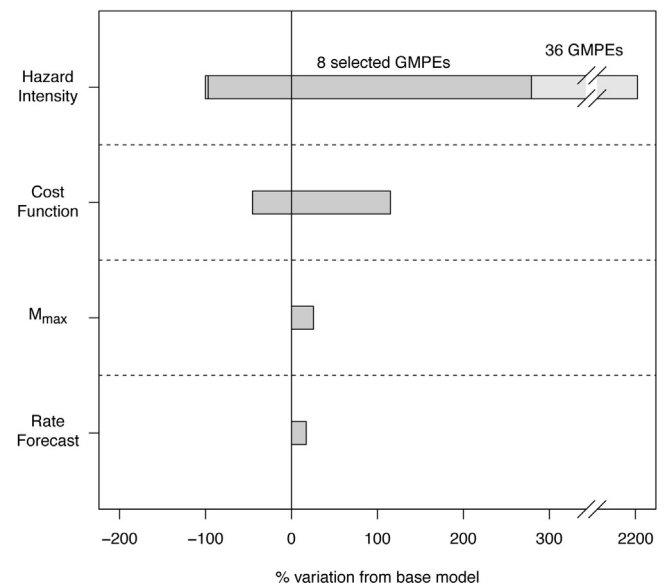


Fig. 8. Tornado plot representing the percentage variation of the MPIVL for different parameters compared to the base model defined by the SERIANEX parameters ($M_{\max} = 3.7$, ECOS-02 IPE and SERIANEX cost function) and the ETASm rate forecast.

the method used to calculate the MPIVL in the present work is simplistic but the overestimation should not have any impact on the analysis of epistemic uncertainties that follows in Section 4. It should be noted that Baisch et al. (2009) obtained a preferred MPIVL = 45,447,835 CHF (median hazard curve, i.e., 0-sigma) and a range 35 millions < MPIVL < 300 millions CHF from a limited exploration of epistemic and aleatory uncertainties. While the numbers are within the distribution shown in Fig. 7b, the range of possibilities is so vast (from 1 million to 600 million CHF) and the assumptions made in the SERIANEX study so different that we could not consider it an agreement between the two analyses. Nevertheless it is worthwhile noting that the SERIANEX estimate is on the upper range of risk estimates (once a more reasonable sigma is included in their hazard integration, i.e. their maximum estimate which is defined by a 85% percentile of the hazard curve), which means that the SERIANEX study led to somewhat pessimistic conclusions.

4. Influence of uncertainties on risk mitigation

4.1. Sensitivity analysis

We identified the parameters whose uncertainty contributes most to the MPIVL variability. We considered the MPIVL as our favourite metric, as it consists of one value per model and includes all tested models, i.e. the 360 possible paths of the logic tree. As indicated by Porter et al. (2002), there are two benefits to knowing the relative contribution of each parameter to the overall uncertainty: (1) the parameters that do not contribute much can reasonably be taken at their best-estimate value, thereby simplifying the analysis by reducing the number of branches in the logic tree and (2) the parameters that do contribute strongly can be investigated in more detail in an attempt to reduce their part in the overall uncertainty (if their part is epistemic uncertainty and not aleatory). Here we use the same approach as in the seismic risk study of Porter et al. (2002), which consists in the ranking of the contributing parameters in a tornado diagram (Fig. 8). We used as base model the SERIANEX parameters ($M_{\max} = 3.7$, ECOS-02 IPE and SERIANEX cost function) and the ETASm rate forecast. For each parameter, the other parameters being fixed to their base value, the two extreme MPIVL values

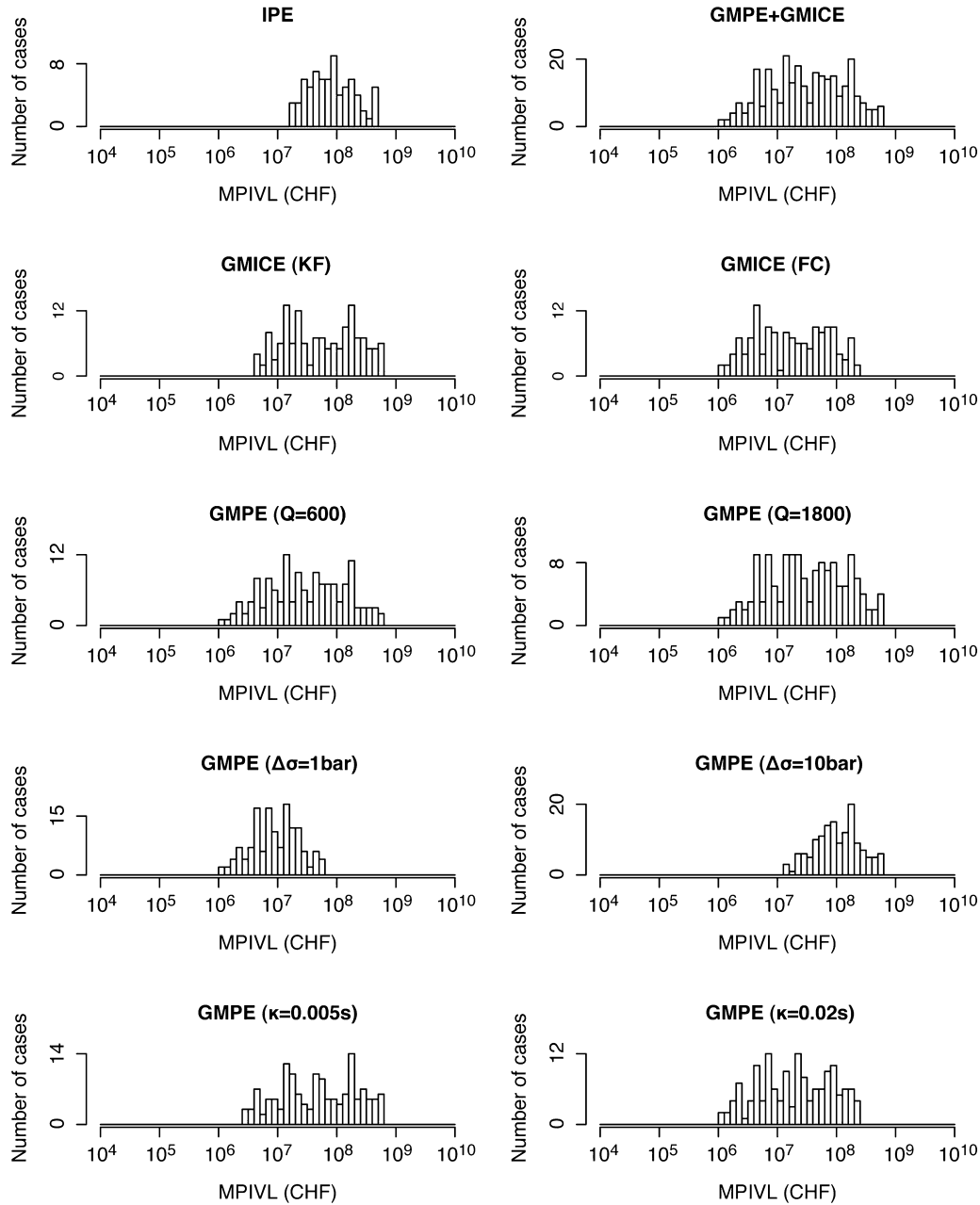


Fig. 9. MPIVL distribution for different GMPE parameter selections. All other parameters vary according to the logic tree structure.

were computed, representing the swing of the tornado diagram – a measure of the sensitivity of the MPIVL to that parameter. We found that hazard intensity models drive the epistemic uncertainty, followed by the cost function, M_{\max} and the rate forecast. While M_{\max} has a limited impact on the overall MPIVL uncertainty for the injection phase (Fig. 8), its role becomes almost as important as the cost function for the post-injection period (not shown). This is due to the decrease of the b -value after shut-in, which means that larger earthquakes become more likely. In both periods, the small impact of forecast models is due to the fact that the 2 tested models (ETASm and Shapiro) were already known to fit well the Basel sequence and because the b -value was calculated in retrospect. In a purely prospective approach, we would expect higher uncertainties associated to the forecast models.

Fig. 8 shows that we had already considerably reduced the contribution of ground motion to the overall loss uncertainty by selecting 8 GMPEs of the 36 proposed by Douglas et al. (2013)

(Fig. 1). Fig. 9 shows that the remaining epistemic uncertainty is mostly controlled by the stress drop value. It remains unclear if the choice of the parameter could still be refined to decrease uncertainties of one order of magnitude or if we are at the limit of inherent variability. The difference in stress drop of the 2006 $M_w = 3.2$ Basel and 2013 $M_w = 3.3$ St Gallen events is a good example of stress drop variability, as while the St Gallen event had a higher magnitude, its stress drop was lower (3 bar versus 10 bar for Basel), which led to felt intensities significantly lower than in Basel (Fig. 3). Finally, the variability related to IPEs is of the same order of the variability related to GMPEs with $\Delta\sigma = 10$ bar.

4.2. Risk mitigation measures

To obtain permission from the regional government of Kanton Basel-Stadt to proceed with the EGS project, a study was required to define an appropriate response procedure in case of increased

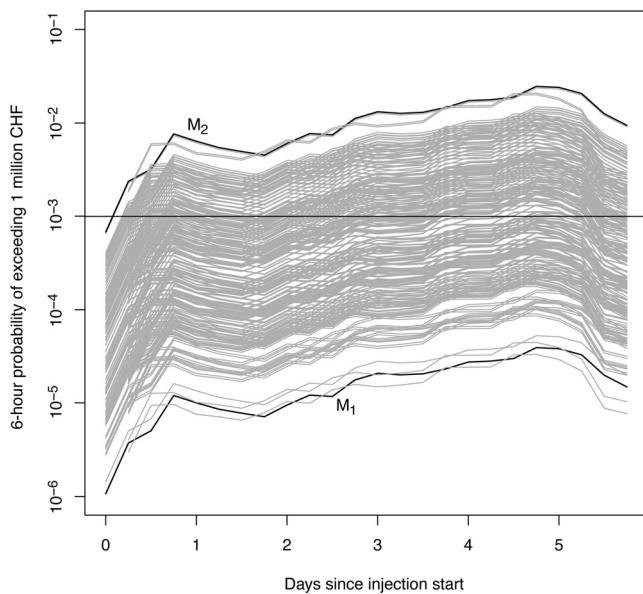


Fig. 10. Probability P of exceeding a 1 million CHF loss at a settlement located at 10 km away from the borehole and over 6-h windows during a repeat of the 6-day Basel stimulation. The 360 ($2 \times 3 \times (4 + 8 \times 2) \times 3$) curves represent the different paths of the logic tree. For illustration purposes, a fictional operator decides to stop injecting fluids when P reaches 10^{-3} . M_1 and M_2 represent two extreme risk models.

seismic activity during the hydraulic stimulation. Häring et al. (2008) described the approach, which is an adaptation of the traffic light system introduced by Bommer et al. (2006) for the Berlin Field (El Salvador) EGS project. In such a system, different levels of action are defined (e.g., no change, pumping at a slower rate, stopping the pump or bleeding the well) depending if a threshold is reached for a given parameter (e.g., event magnitude, macroseismic intensity, PGV, public response), be it observed or forecasted (Bachmann et al., 2011; Mena et al., 2013). Here we investigated the influence of uncertainties on induced seismicity risk mitigation by developing a risk-based traffic light system similar to the approach used at the hazard level by Mena et al. (2013). We considered the probability P of exceeding a 1 million CHF loss at a settlement located at 10 km away from the borehole and over 6-h windows during a repeat of the 6-day Basel stimulation. Fig. 10 shows the evolution of P over time for the 360 proposed model options. For simplicity reasons, let us assume that a fictional operator decides to stop injecting fluids when P reaches 10^{-3} . It is important to note that this traffic light system is only proposed for illustration purposes and that we do not make any recommendation as to which metric or threshold should be used.

The following discussion is based on results obtained from the theory of decision-making under uncertainty (Gilboa, 2009; Walker and Dietz, 2012). We first make the distinction between the terms risk and ambiguity, risk corresponding to precise probabilities (Knight, 1921) while ambiguity expresses epistemic uncertainty. Since this aspect is rarely, if at all addressed in EGS traffic light systems (Bommer et al., 2006; Häring et al., 2008; Convertito et al., 2012), we used results from the broad literature of economics of climate change, in which benefit-cost analyses also depend on large epistemic uncertainties (Woodward and Bishop, 1997; Dietz, 2012; Heal and Millner, 2013). Although a simple averaging of the estimates of the different models may appear attractive, the theory of decision-making under uncertainty cautions against such an approach. Following the Principle of Insufficient Reason, one would place equal weights to all models. However Woodward and Bishop (1997) among many others indicated that this approach provides more weight to an outcome if several models yield the

same outcome despite not knowing which model is best. Adding other models, which outcome is already considered, should have no impact on the final decision meaning that it is the minimum and maximum outcomes that count. In that view, one must minimize the possible maximum losses (worst case scenario) or maximize the possible minimum gains (i.e., criteria of Minimax and Maximin). Noteworthy, worst case scenarios drive overall willingness to pay for mitigation. This is due to ambiguity aversion, which means that pessimistic models are preferred. A decision maker can however react to ambiguity in different ways: he can be ambiguity averse, ambiguity neutral or ambiguity seeking. Therefore decision becomes subjective but this subjectivity is known of the decision maker and its interlocutors, which avoids potential misunderstanding of the treatment of risk and its uncertainty. As indicated by Heal and Millner (2013), the fact that many people are ambiguity averse does not mean that ambiguity aversion is rational, and should form part of normative policy analysis. For example, the Maximax criterion corresponds to the optimistic view in which one maximizes the possible maximum gains. Finally based on simple climate change scenarios, Woodward and Bishop (1997) demonstrated that the policies that assume the worst at the outset are more robust than relatively optimistic scenarios but that adjustments should be made if information on model likelihood comes to light over time.

Although mitigation of climate change and of induced seismicity in an EGS are two distinct problems, we provide a few recommendations on how to treat epistemic uncertainty in the proposed traffic light represented in Fig. 10, based on lessons learned from climate change risk management. We originally assumed – due to lack of knowledge – that all models have the same weight. In that view, each curve represents a quantile of the distribution and one may choose to make a decision based on a specific quantile, for instance the median. This choice, if clearly stated, could be used to respond to official regulations, such as building norms in which a specific PGV threshold should not be exceeded. Let us however extend the discussion on the possible treatment of uncertainties.

If we follow the theory of decision-making under uncertainty, a criterion based on extreme outcomes should be preferred. The outcome depends not only on the induced seismicity risk represented in Fig. 10 but also on the inherent project losses (e.g., drilling costs) and possible gains (i.e., energy production) depending on the duration of the injection/circulation phase. Such an analysis is out of the scope of the present study. Nevertheless, the following illustration shows the steps that operators may decide to take in future EGS projects to better integrate uncertain outcomes. Let us consider a set of 2 actions A and a set of 2 states S . The outcome of a

Table 3

Illustration of decision-making under uncertainty in a payoff table. Action A_1 and state S_1 are based on the minimum risk model M_1 and A_2 and S_2 on the maximum risk model M_2 . Losses L and gains G are defined following the traffic light system shown in Fig. 10, with $L_1 < L_2$ for A_1 and $G_2 = L_1 = L_2 = 0$ for A_2 .

	S_1	S_2	Minimax/Maximin	Maximax
A_1	$G_1 - L_1$	$G_1 - L_2$		
A_2	$G_2 - L_1$	$G_2 - L_2$		
$G_1 < L_1 < L_2$				
A_1	–	–		
A_2	0	0	✓	✓
$L_1 < G_1 < L_2$				
A_1	+	–		
A_2	0	0	✓	✓
$L_1 < L_2 < G_1$				
A_1	++	+	✓	
A_2	0	0		✓

given action depends upon the state that results. Action A_1 is based on the minimum risk model M_1 , meaning that the injection never stops (Fig. 10) and that G_1 gains are made. Action A_2 is based on the maximum risk model M_2 , meaning that the injection immediately stops (Fig. 10) and therefore that no gain is made ($G_2 = 0$). States S_1 and S_2 correspond to losses L_1 (model M_1 true) and L_2 (model M_2 true), respectively, with $L_1 < L_2$. It should be noted that the state also depends on the action. Therefore $L_1 = L_2 = 0$ for A_2 . Table 3 shows the different actions to be preferred in the Minimax/Maximin (pessimistic) and Maximax (optimistic) views for different values of G_1 relative to L_1 and L_2 . An action can here be interpreted as a “bid against Nature”, as defined in Game Theory. While Maximin and Minimax are the same here, it may not always be the case. We find that the Minimax/Maximin criterion favours action A_2 compared to the Maximax, which favours action A_1 . However both criteria yield similar outcomes for cases where the difference between gains and losses is clear (e.g., all gain $L_1 < L_2 < G_1$ versus all loss $G_1 < L_1 < L_2$). In a more realistic case, one could consider up to 360 actions and 360 states based on the results of Fig. 10.

Finally, model selection should be updated over time when more information becomes available. In the case of EGSs, forecast models can already be adjusted throughout an induced seismicity sequence (Mena et al., 2013) and it has been proposed to do the same for GMPE models (Douglas et al., 2013). Prospective forecasting of the most sensitive parameters should in principle improve decision-making over time by reducing the number of scenarios shown in Fig. 10.

5. Conclusions

We presented a probabilistic seismic risk analysis of the 2006 Basel EGS project by combining time-dependent forecast models to the RISK-UE macroseismic approach for risk assessment. Using a logic tree approach, we calculated the sensitivity of risk estimates to different input parameters and showed that results vary over several orders of magnitude based on the proposed logic tree. To our knowledge, the present study is the first one to consider uncertainties at the hazard and risk levels in a systematic way in the scope of induced seismicity regimes. We showed that the SERIANEX study (Baisch et al., 2009), by consciously not considering epistemic

uncertainties, led to subjective – rather high – risk estimates, based on which the Basel EGS project was terminated. While thorough in some respects, we showed that the SERIANEX study did not explore the full risk distribution, based on which alternative decisions may have been taken.

We showed that epistemic uncertainties are mostly controlled by the choice of GMPEs. Although the impact can be reduced by selecting models that satisfy regional conditions, scattering remains consequent. Future studies should aim at better understanding the origin of GMPE parameter variability (e.g., induced earthquake stress drop) and if it can still be reduced. Adjustment of the GMPE parameters over time in the case of traffic light systems should also be explored.

Decision-making under uncertainty remains almost inexistent in EGSs although different models may lead to very different mitigation actions. Based on the climate change literature and using a simple EGS traffic light system, we discussed the main strategies to make reliable decisions when ambiguous results are available. We showed that averaging and equal weighting should be avoided and that a ranking of cost-benefit options should be made to cope with the worst possible scenario. These basic concepts have yet to be tested.

Acknowledgments

We thank Julian Bommer and an anonymous reviewer for their constructive comments. We are also grateful to Clotaire Michel for helping us estimate V_i ranges when not available in the literature and to Benjamin Edwards for discussions on GMPEs. Finally, we are indebted to the SERIANEX team for making their risk analysis public. This research was supported by the FP7 project Geothermal Engineering Integrating Mitigation of Induced Seismicity in Reservoirs (GEISER), Grant Agreement Number 241321-2, and by the CCES project GEOTHERM.

Appendix: Basel building stock.

This appendix gives the characteristics of the Basel building stock (Tables A1–A3). More details can be found in the SERIANEX report (Baisch et al., 2009).

Table A1

Basel building stock. Co.: Country; # build.: number of buildings (Baisch et al., 2009); IV/build.: average insured value in CHF per building (Baisch et al., 2009); x, y: Swiss coordinates in km (swisstopo, 2012).

No.	Name	Co.	# build.	IV/build.	x	y
1	Basel, Grossbasel	CH	491	2,409,010	611,275	267,340
2	Basel, Kleinbasel	CH	282	2,409,010	611,615	267,760
3	Basel, Vorstädte	CH	565	2,409,010	611,290	266,850
4	Basel, Am Ring	CH	1174	2,409,010	610,516	267,337
5	Basel, Breite	CH	653	2,409,010	613,390	266,930
6	Basel, St. Alban	CH	1190	2,409,010	612,700	266,200
7	Basel, Gundeldingen	CH	1411	2,409,010	611,711	265,795
8	Basel, Bruderholz	CH	2031	2,409,010	611,775	264,684
9	Basel, Bachletten	CH	2467	2,409,010	609,869	266,502
10	Basel, Gotthelf	CH	968	2,409,010	609,910	267,182
11	Basel, Iselin	CH	1444	2,409,010	609,804	267,861
12	Basel, St. Johann	CH	1520	2,409,010	610,241	268,943
13	Basel, Clara	CH	251	2,409,010	611,831	268,174
14	Basel, Wettstein	CH	673	2,409,010	612,459	267,835
15	Basel, Hirzbrunnen	CH	1524	2,409,010	613,126	268,640
16	Basel, Rosental	CH	255	2,409,010	612,332	268,545
17	Basel, Matthäus	CH	1116	2,409,010	611,580	268,575
18	Basel, Kleinhüningen	CH	164	2,409,010	611,575	270,360
19	Basel, Klybeck	CH	437	2,409,010	611,494	269,594
20	Aesch	CH	1891	1,312,827	611,996	257,387.1
21	Allschwil	CH	3131	1,482,827	607,323	266,713
22	Arlesheim	CH	1756	1,522,203	613,699	260,186
23	Bättwil	CH	268	1,753,199	605,392.7	259,902.4
24	Bettingen	CH	276	1,753,199	617,043	268,959
25	Biel-Benken	CH	841	1,025,803	606,514	261,812
26	Binningen	CH	2652	1,463,020	610,012.7	265,145
27	Birsfelden	CH	1072	2,279,875	614,025.9	266,820
28	Bottmingen	CH	1464	1,075,839	610,140	263,615
29	Dornach	CH	1418	1,573,261	613,526	258,726
30	Ettingen	CH	1125	922,919	608,016.3	258,949.2
31	Frenkendorf	CH	1058	1,300,099	620,853.8	261,438.4
32	Kaiseraugst	CH	468	1,753,199	621,650	265,220
33	Münchenstein	CH	2514	1,547,883	613,684.2	262,437.8
34	Muttenz	CH	3453	1,865,587	615,320	264,470
35	Oberwil	CH	2233	1,166,933	608,978.1	262,719.6
36	Pratteln	CH	2322	1,874,758	619,040	263,560
37	Reinach	CH	3889	1,232,005	611,484	260,348
38	Riehen	CH	3894	1,436,149	615,730	269,790
39	Schönenbuch	CH	397	1,753,199	604,772.8	265,174.8
40	Therwil	CH	2031	1,048,072	608,678.4	260,902.6
41	Witterswil	CH	427	1,753,199	606,354.3	259,456.3
42	Binzen	DE	778	1,573,261	613,815	275,720
43	Efringen-Kirchen	DE	2229	1,504,142	609,620.8	277,713.7
44	Eimeldingen	DE	510	1,573,261	611,800	275,700
45	Fischingen	DE	201	1,573,261	612,125.3	277,718.3
46	Grenzach-Wyhlen	DE	2929	1,372,331	617,166.5	266,611.6
47	Inzlingen	DE	657	1,573,261	618,780	270,900
48	Lörrach	DE	7730	1,504,142	616,800	273,420
49	Rümmingen	DE	452	1,753,199	615,430	276,830
50	Schallbach	DE	203	1,753,199	614,120	278,500
51	Steinen	DE	2342	1,372,331	622,635	277,100
52	Weil am Rhein	DE	5278	1,504,142	614,240	271,475
53	Wittlingen	DE	261	1,753,199	615,840	278,450
54	Attenschwiller	FR	339	1,753,199	601,800	268,425
55	Bartenheim	FR	1402	1,573,261	602,890	275,970
56	Blotzheim	FR	1568	1,573,261	604,340	272,330
57	Brinckheim	FR	130	1,753,199	601,520	275,100
58	Buschwiller	FR	367	1,753,199	605,225	267,580
59	Folgenbourg	FR	287	1,753,199	600,425	266,570
60	Hagenthal-le-Bas	FR	399	1,753,199	603,000	263,850
61	Hagenthal-le-Haut	FR	173	1,753,199	602,250	263,200
62	Hégenheim	FR	1084	1,573,261	606,570	267,880
63	Helfrantzkirch	FR	297	1,573,261	598,195	272,780
64	Hésingue	FR	786	1,573,261	606,100	269,425
65	Huningue	FR	2981	1,372,331	610,800	271,510
66	Kappelen	FR	194	1,753,199	599,825	274,215
67	Kembs	FR	1579	1,573,261	604,608.9	281,414.2
68	Michelbach-le-Bas	FR	284	1,753,199	601,915	271,300
69	Michelbach-le-Haut	FR	188	1,753,199	600,350	268,340
70	Neuwiller	FR	219	1,753,199	605,805	263,715
71	Ranspach-le-Bas	FR	271	1,753,199	600,460	270,755
72	Ranspach-le-Haut	FR	177	1,753,199	598,525	269,590
73	Rosenau	FR	793	1,753,199	607,240	276,250
74	Saint-Louis	FR	8889	1,504,142	609,632.8	270,301
75	Sierentz	FR	1032	1,573,261	601,235	278,000
76	Stetten	FR	111	1,753,199	598,955	274,820
77	Uffheim	FR	335	1,753,199	600,290	277,660
78	Village-Neuf	FR	1475	1,573,261	609,840	272,860
79	Wentzwiller	FR	226	1,753,199	603,075	266,550

Table A2

Number of buildings per building class, derived from [Baisch et al. \(2009\)](#). The first column (No.) refers to the settlement names given in [Table A1](#). Building classes are explained in [Table A3](#).

No.	M1	M2	M3	M4	M5	M6	M7	RC1	RC2	RC3	RC4	RC5	S1	S2	W1	W2
1	302.3	33.4	22.8	0	6.8	0	6.8	0	35.55	3.95	20.4	15.4	6.3	0	0	37.3
2	135.2	14.2	26.2	0	5.2	0	5.2	0	36.35	3	15.6	17	6.45	0	0	16.6
3	224	0	88.35	73.6	0	0	0	0	90.35	7.6	11.2	40.4	15.9	13.6	0	0
4	498.9	0	169.15	155.65	0	0	0	0	178.65	14.85	21.8	80.8	29.95	24.25	0	0
5	123.3	11.7	31.05	0	36.8	0	36.8	0	150.14	7.5	110.4	87.90	42.4	0	0	15
6	283.8	0	412.65	63.4	0	0	0	0	194.65	16.65	79.4	92	39.25	8.2	0	0
7	444.2	52.6	94.7	0	70.8	0	70.8	0	236.6	20.9	212.4	109.4	43.4	0	0	55.2
8	74	0	826.9	1.6	239	0	239	0	182.4	63.7	396	0	0	0	0	8.4
9	357.2	22.6	232.6	0	279	0	279	0	211.7	9.8	837	130.6	65.3	0	0	42.2
10	263.6	24.4	17.95	0	93.2	0	93.2	0	89.5	7.6	279.6	52	14.95	0	0	32
11	298	25.1	47.85	0	102.8	0	102.8	0	268.85	13	308.4	163.5	77.8	0	0	35.9
12	393.5	39.4	85.2	0	109.4	0	109.4	0	224.8	18	328.2	111.2	52.8	0	0	48.1
13	81.5	0	42.9	27.15	0	0	0	0	52.85	4.8	5	23.4	8.05	5.35	0	0
14	188.7	0	249.45	42.35	0	0	0	0	70.5	7.35	61	32.3	14.5	6.95	0	0
15	25.6	2.3	120.45	0	221	0	221	0	134.6	5.65	663	84.7	42.6	0	0	3.1
16	48.1	5.9	9.45	0	17.2	0	17.2	0	55.05	4	51.6	28.7	11.8	0	0	6
17	471.2	51.7	73.25	0	21.4	0	21.4	0	203.5	17.05	64.2	94.3	39.9	0	0	58.1
18	21.2	2.2	6.7	0	7.2	0	7.2	0	49.05	2.95	21.6	31.3	12	0	0	2.6
19	103.5	10.8	11.9	0	26	0	26	0	86.15	4.75	78	54.1	23.1	0	0	12.7
20	83	0	1017.15	0	79.5	0	79.5	0	148.7	381.9	0	0	0	0	18.25	83
21	304.4	70.6	1348.66	248.9	136.5	0	0	0	362.4	484.95	0	23.85	9.54	0	0	141.2
22	130	0	785.85	0	155	0	155	0	136.45	249.8	0	0	0	0	13.9	130
23	12	0	134.35	0	4.5	0	4.5	0	25.35	67.8	0	0	0	0	7.5	12
24	11.5	0	149	0	14	0	14	0	19.3	53.8	0	0	0	0	2.9	11.5
25	37.5	0	492.35	0	11.5	0	11.5	0	68.75	230.7	0	0	0	0	14.2	37.5
26	336.5	35	1206.3	239.5	60.5	0	0	0	200.8	355.2	0	47.6	13.1	0	0	157.5
27	108.5	0	322.05	0	156	0	156	0	125	93.85	0	0	0	0	2.1	108.5
28	47.5	0	835.6	0	47	0	47	0	98.4	322.55	0	0	0	0	18.45	47.5
29	84.5	0	661.95	0	120.5	0	120.5	0	102.3	231.15	0	0	0	0	12.6	84.5
30	57.5	0	615.55	0	16	0	16	0	84.75	265.85	0	0	0	0	11.85	57.5
31	56.5	0	534.45	0	60	0	60	0	94.85	184.35	0	0	0	0	11.35	56.5
32	27	0	211.95	0	21.5	0	21.5	0	62.3	90.5	0	0	0	0	6.25	27
33	394.25	28.5	1089.3	320	54	0	0	0	165.43	296.85	0	29.3	8.12	0	0	128.25
34	269	53.2	1848.81	226.6	86.1	0	0	0	318.65	513.65	0	21.85	8.74	0	0	106.4
35	140	19	1239.2	67	12.5	0	0	0	165.36	452	0	40.95	11.49	0	0	85.5
36	297.15	32.7	1015.1	200	50	0	0	0	193.84	308.25	0	61.75	16.06	0	0	147.15
37	128.2	29	2268.49	94.2	28.7	0	0	0	396	842.45	0	31.4	12.56	0	0	58
38	341.2	57.2	2028.5	310.2	106.4	0	0	0	413.6	490.65	0	22.75	9.1	0	0	114.4
39	16	0	210.4	0	7	0	7	0	30.45	101.3	0	0	0	0	8.85	16
40	79.6	10.8	1184.8	36	5	0	0	0	148.74	467.9	0	39.15	10.41	0	0	48.6
41	21.5	0	233.4	0	7	0	7	0	23.75	105.3	0	0	0	0	7.55	21.5
42	63.6	2	53.8	30.8	234.4	0	0	0	74.7	324	0	22.9	0	0	0	30.8
43	255.9	6.45	168.9	121.5	515.9	0	0	0	221.1	754.8	0	62.95	0	0	0	121.5
44	42.95	2.95	41.9	20	127.95	0	0	0	54	185.2	0	15.05	0	0	0	20
45	21.7	0	17.1	10.4	53	0	0	0	17.1	70.4	0	0.9	0	0	0	10.4
46	257.2	10.4	253.4	123.4	646.6	0	0	0	348.9	1059.8	0	105.9	0	0	0	123.4
47	70.54	1.77	58.3	33.5	134.04	0	0	0	78.6	223.5	0	23.25	0	0	0	33.5
48	466.35	17.55	634.50	224.4	1407.7	0	0	0	1198.8	2848.15	0	469.8	182.25	0	0	280.5
49	38.65	0	44.4	18.6	117.7	0	0	0	44.4	168.2	0	1.45	0	0	0	18.6
50	21.8	0	17.4	10.5	53.1	0	0	0	17.4	71.5	0	0.8	0	0	0	10.5
51	221.08	5.34	206.4	105.2	499.78	0	0	0	282.9	830.7	0	85.4	0	0	0	105.2
52	410.76	5.8	313.25	202.48	1209.03	0	0	0	603.3	1961.23	0	224.3	94.75	0	0	253.1
53	22.1	0	23.4	10.5	72.7	0	0	0	23.4	97.3	0	1.1	0	0	0	10.5
54	23	0	174.35	23	23	0	0	0	0	46.5	0	17.15	0.3	0	8.7	23
55	71	14.2	678.72	56.8	71	0	0	0	0	175.7	0	233.8	5.28	0	24.5	71
56	78.5	15.7	797.4	62.8	78.5	0	0	0	0	199.5	0	226.5	2.9	0	27.7	78.5
57	8.75	0	70.38	8.75	8.75	0	0	0	0	20.3	0	0.7	0.02	0	3.6	8.75
58	21.75	0	194.03	21.75	21.75	0	0	0	0	46.9	0	30.55	0.52	0	8	21.75
59	17.75	0	150.53	17.75	17.75	0	0	0	0	33.6	0	37.25	0.82	0	5.8	17.75
60	22	0	205.56	22	22	0	0	0	0	43.7	0	55	1.14	0	5.6	22
61	15	0	84.85	15	15	0	0	0	0	22.7	0	1.95	0	0	3.5	15
62	80.75	16.15	503.6	64.6	80.75	0	0	0	0	127.5	0	114.5	1.9	0	13.5	80.75
63	23.25	0	150.81	23.25	23.25	0	0	0	0	41.1	0	5.85	0.14	0	6.1	23.25
64	54.25	10.85	379.4	43.4	54.25	0	0	0	0	95	0	84	1.4	0	9.2	54.25
65	148.5	29.7	1190.68	118.8	148.5	0	0	0	0	109	0	1073.8	8.52	0	5	148.5
66	12	0	98.46	12	12	0	0	0	0	24.2	0	18.6	0.44	0	4.3	12
67	57	11.4	902.62	45.6	57	0	0	0	0	274.6	0	126.3	2.48	0	45	57
68	10.5	0	180.44	10.5	10.5	0	0	0	0	48.4	0	5.1	0.06	0	8	10.5
69	12.25	0	104.31	12.25	12.25	0	0	0	0	23.1	0	9.05	0.14	0	2.4	12.25
70	14	0	121.38	14	14	0	0	0	0	30	0	7	0.02	0	4.6	14
71	18	0	135.26	18	18	0	0	0	0	31.5	0	26.4	0.74	0	5.1	18
72	13.25	0	89.58	13.25	13.25	0	0	0	0	27.1	0	2.2	0.02	0	5.1	13.25
73	23	4.6	459.9	18.4	23	0	0	0	0	134.4	0	82.5	2.2	0	19	23
74	293.94	244.95	2168.15	277.61	408.25	0	0	118.2	0	1030	0	3807.6	107.05	0	25	408.25
75	61.5	12.3	450.48	49.2	61.5	0	0	0	0	100.7	0	218.2	4.72	0	11.9	61.5
76	10.25	0	50.32	10.25	10.25	0	0	0	0	13.8	0	3.8	0.08	0	2	10.25
77	19.5	0	179.17	19.5	19.5	0	0	0	0	45.2	0	25.55	0.58	0	6.5	19.5
78	92.75	18.55	653.92	74.2	92.75	0	0	0	0	142.4	0	287.3	5.38	0	15	92.75
79	17.5	0	113.36	17.5	17.5	0	0	0	0	27.4	0	10.4	0.24	0	4.6	17.5

Table A3

SERIANEX building classes (BC_{SER}) (Baisch et al., 2009). Match with EMS-98 classes (BC_{EMS}) is made when evident (Grünthal, 1998). V0 values were defined by Baisch et al. (2009) while $V+/V-$ and $V-+/V++$ values were defined in the present study. For building classes that coincide with EMS-98 classes, EMS-98 values were taken (Lagomarsino and Giovinazzi, 2006). For Basel-specific classes, we oriented ourselves to similar values given in the EMS-98 classification to obtain reasonable (while always debatable) estimates of the $V+/V-$ and $V-+/V++$ unknown ranges. EMS-98 vulnerability classes (VC_{EMS}) required for casualty estimations were obtained by using the membership functions, which can be found in Lagomarsino and Giovinazzi (2006).

Building class				VC_{EMS}	Vulnerability index				
	BC_{SER}	Type of structure	BC_{EMS}		$V-/-$	$V-/-$	V0	$V+/+$	$V++$
Masonry (M)	M1	Simple stone with timber slabs	M3	B	0.46	0.65	0.74	0.83	1.02
	M2	Massive stone with timber slabs	M4	C	0.3	0.49	0.616	0.793	0.86
	M3	Brick with concrete slabs	M6	C	0.3	0.49	0.616	0.79	0.86
	M4	Simple stone with hollow-core slabs	–	B	0.42	0.61	0.7	0.79	0.9
	M5	Brick with hollow-core slabs	–	C	0.32	0.5	0.65	0.8	0.87
	M6	Massive stone with hollow-core slabs	–	C	0.32	0.5	0.65	0.8	0.87
	M7	Brick with timber slabs	M3	B	0.46	0.65	0.74	0.83	1.02
Reinforced concrete (RC)	RC1	Concrete moment frames	–	D	0.14	0.207	0.442	0.64	0.86
	RC2	Concrete shear walls	RC5	D	0.14	0.21	0.386	0.51	0.7
	RC3	Concrete walls and brick masonry walls	–	D	0.15	0.22	0.4	0.52	0.71
	RC4	Hennebique system ^a	–	C	0.25	0.3	0.5	0.7	0.85
	RC5	Concrete moment frames with infills	–	D	0.15	0.22	0.402	0.52	0.71
Steel (S)	S1	Steel structures (moment and brace F)	S	E	–0.02	0.17	0.325	0.48	0.7
	S2	Old steel structures	–	D	0.15	0.22	0.4	0.52	0.71
Wood (W)	W1	Timber structures	W	D	0.14	0.207	0.447	0.64	0.86
	W2	Half-timbered structures	–	D	0.17	0.24	0.48	0.67	0.89

^a Hennebique system: construction system developed by French engineer F. Hennebique (1842–1921), which belongs to the first generation of reinforced concrete structures (read more in Baisch et al., 2009).

References

- Allen, T.I., Wald, D.J., Worden, C.B., 2012. Intensity attenuation for active crustal regions. *J. Seismol.* 16, 409–433. <http://dx.doi.org/10.1007/s10950-012-9278-7>.
- Alvarez-Rubio, S., Kästli, P., Fäh, D., Sellami, S., Giardini, D., 2012. Parameterization of historical earthquakes in Switzerland. *J. Seismol.* 16, 1–24. <http://dx.doi.org/10.1007/s10950-011-9245-8>.
- Bachmann, C.E., Wiemer, S., Woessner, J., Hainzl, S., 2011. Statistical analysis of the induced Basel 2006 earthquake sequence: introducing a probability-based monitoring approach for Enhanced Geothermal Systems. *Geophys. J. Int.* 186, 793–807.
- Baisch, S., Carbon, D., Dannwolf, U., Delacou, B., Devaux, M., Dunand, F., Jung, R., Koller, M., Martin, C., Sartori, M., 2009. Deep Heat Mining Basel: Seismic Risk Analysis, SERIANEX Group. Departement für Wirtschaft, Soziales und Umwelt des Kantons Basel-Stadt, Basel.
- Baisch, S., Vörös, R., Rothert, E., Stang, H., Jung, R., Schellschmidt, R., 2010. A numerical model for fluid injection induced seismicity at Soultz-sous-Forêts. *Int. J. Rock Mech. Mining Sci.* 47, 405–413. <http://dx.doi.org/10.1016/j.ijrmms.2009.10.001>.
- Barth, A., Wenzel, F., Langenbruch, C., 2013. Probability of earthquake occurrence and magnitude estimation in the post shut-in phase of geothermal projects. *J. Seismol.* 17, 5–11.
- Bommer, J.J., Abrahamson, N.A., 2006. Why do modern probabilistic seismic-hazard analyses often lead to increased hazard estimates? *Bull. Seismol. Soc. Am.* 96, 1967–1977. <http://dx.doi.org/10.1785/0120060043>.
- Bommer, J.J., Oates, S., Cepeda, J.M., Lindholm, C., Bird, J., Torres, R., Marroquin, G., Rivas, J., 2006. Control of hazard due to seismicity induced by a hot fractured rock geothermal project. *Eng. Geol.* 83, 287–306. <http://dx.doi.org/10.1016/j.enggeo.2005.11.002>.
- Brown, D.W., Duchane, D.V., Heiken, G., Hrisu, V.T., 2012. Mining the Earth's Heat: Hot Dry Rock Geothermal Energy. Springer, <http://dx.doi.org/10.1007/978-3-540-68910-2>.
- Charl  t  , J., Cuenot, N., Dorbath, L., Dorbath, C., Haessler, H., Frogneux, M., 2007. Large earthquakes during hydraulic stimulations at the geothermal site of Soultz-sous-For  ts. *Int. J. Rock Mech. Mining Sci.* 44, 1091–1105. <http://dx.doi.org/10.1016/j.ijrmms.2007.06.003>.
- Cochrane, S., Shaad, W., 1992. Assessment of earthquake vulnerability of buildings. In: Paper presented at Earthquake Engineering, 10th World Conference, Balkema, Rotterdam.
- Convertito, V., Maercklin, N., Sharman, N., Zollo, A., 2012. From induced seismicity to direct time-dependent seismic hazard. *Bull. Seismol. Soc. Am.* 102, 2563–2573. <http://dx.doi.org/10.1785/0120120036>.
- Cornell, C., 1968. Engineering seismic risk analysis. *Bull. Seismol. Soc. Am.* 59, 1583–1606.
- Crowley, H., Pinho, R., Bommer, J.J., 2004. A probabilistic displacement-based vulnerability assessment procedure for earthquake loss estimation. *Bull. Earthquake Eng.* 2, 173–219.
- Crowley, H., Bommer, J.J., Pinho, R., Bird, J., 2005. The impact of epistemic uncertainty on an earthquake loss model. *Earthquake Eng. Struct. Dyn.* 34, 1653–1685.
- Crowley, H., Bommer, J.J., 2006. Modelling seismic hazard in earthquake loss models with spatially distributed exposure. *Bull. Earthquake Eng.* 4, 249–273. <http://dx.doi.org/10.1007/s10518-006-9009-y>.
- Dietz, S., 2012. The treatment of risk and uncertainty in the US social cost of carbon for regulatory impact analysis. *Economics* 6, <http://dx.doi.org/10.5018/economics-ejournal.ja.2012-18>.
- Douglas, J., Edwards, B., Convertito, V., Sharma, N., Tramel, A., Kraaijpoel, D., Mena Cabrera, B., Maercklin, N., Troise, C., 2013. Predicting ground motion from induced earthquakes in geothermal areas. *Bull. Seismol. Soc. Am.* (accepted February 2013).
- Edwards, B., F  h, D., 2013. A stochastic ground-motion model for Switzerland. *Bull. Seismol. Soc. Am.* 103, 78–98. <http://dx.doi.org/10.1785/0120110331>.
- Esteva, L., 1970. Seismic risk and seismic design decisions. In: Hansen, R.J. (Ed.), *Seismic Design for Nuclear Power Plants*. MIT Press, Cambridge, MA, pp. 142–182.
- Evans, K.F., Zappone, A., Kraft, T., Deichmann, N., Moia, F., 2012. A survey of the induced seismic responses to fluid injection in geothermal and CO₂ reservoirs in Europe. *Geothermics* 41, 30–54. <http://dx.doi.org/10.1016/j.geothermics.2011.08.002>.
- Facciolo, E., Cauzzi, C., 2006. Macroseismic intensities for seismic scenarios, estimated from instrumentally based correlations. In: 1st European Conf. Earthquake Engineering and Seismology, 3–8 September 2006, Geneva, Switzerland, p. 569.
- F  h, D., Giardini, D., Bay, F., Bernardi, F., Braunmiller, J., Deichmann, N., Furrer, M., Gantner, L., Gisler, M., Isenegger, D., Jimenez, M.J., K  stli, P., Koglin, R., Masciadri, V., Rutz, M., Scheidegger, C., Schibler, R., Schorlemmer, D., Schwarz-Zanetti, G., Steinen, S., Sellami, S., Wiemer, S., W  ssner, J., 2003. Earthquake Catalogue Of Switzerland (ECOS) and the related macroseismic database. *Eclogae Geol. Helv.* 96, 219–236. <http://dx.doi.org/10.1007/s00015-003-1087-0>.
- F  h, D., K  stli, P., Alvarez, S., Poggi, V., 2010. Intensity data from the MECOS database. In: Schweizerischer Erdbebendienst ETH Zurich, Report SED/PRP/R/012/20100607.
- F  h, D., Giardini, D., K  stli, P., Deichmann, N., Gisler, M., Schwarz-Zanetti, G., Alvarez-Rubio, S., Sellami, S., Edwards, B., Allmann, B., Bethmann, F., W  ssner, J., Gassner-Stamm, G., Fritsche, S., Eberhard, D., 2011. ECOS-09 Earthquake Catalogue of Switzerland Release 2011. In: Report and Database, Public catalogue, 17.4.2011, Swiss Seismological Service ETH Z  rich, Report SED/RISK/R/001/20110417.
- Gerstenberger, M.C., Wiemer, S., Jones, L.M., Reasenber, P.A., 2005. Real-time forecasts of tomorrow's earthquakes in California. *Nature* 435, 328–331. <http://dx.doi.org/10.1038/nature03622>.
- Giardini, D., 2009. Geothermal quake risks must be faced. *Nature* 462, 848–849.
- Gilboa, I., 2009. *Theory of Decision under Uncertainty*. Cambridge University Press, Cambridge, UK.
- Goertz-Allmann, B.P., Wiemer, S., 2013. Geomechanical modeling of induced seismicity source parameters and implications for seismic hazard assessment. *Geophysics* 78, <http://dx.doi.org/10.1190/GEO2012-0102.1>.
- Gr  nthal, G. (Ed.), 1998. European Macroseismic Scale 1998 (EMS-98). *Cahiers du Centre Europ  en de G  odynamique et de S  ismologie* 15. Centre Europ  en de G  odynamique et de S  ismologie, Luxembourg, p. 99.
- Gr  nthal, G., Wahlstr  m, R., 2012. The European-Mediterranean Earthquake Catalogue (EMEC) for the last millennium. *J. Seismol.* 16, 535–570.
- Gutenberg, B., Richter, C.F., 1944. Frequency of earthquakes in California. *Bull. Seismol. Soc. Am.* 34, 184–188.

- Häring, M.O., Schanz, U., Ladner, F., Dyer, B.C., 2008. *Characterisation of the Basel 1 enhanced geothermal system*. *Geothermics* 37, 469–495.
- Heal, G., Millner, A., 2013. *Uncertainty and decision in climate change economics*. Grantham Research Institute on Climate Change and the Environment, Working Paper No. 108.
- Horton, S., 2012. Disposal of hydrofracking waste fluid by injection into subsurface aquifers triggers earthquake swarm in Central Arkansas with potential for damaging earthquake. *Seismol. Res. Lett.* 83, 250–260, <http://dx.doi.org/10.1785/gssrl.83.2.250>.
- Kästli, P., Fäh, D., 2006. *Rapid estimation of macroseismic effects and Shakesmaps using macroseismic data*. In: First European Conference on Earthquake Engineering and Seismology, Geneva.
- Knight, F.H., 1921. *Risk, Uncertainty and Profit*. Houghton Mifflin, Boston.
- Kraft, T., Mai, P.M., Wiemer, S., Deichmann, N., Ripperger, J., Kästli, P., Bachmann, C., Fäh, D., Wössner, J., Giardini, D., 2009. *Enhanced geothermal systems: mitigating risk in urban areas*. *Eos* 90, 273–280.
- Kulkarni, R.B., Youngs, R.R., Coppersmith, K.J., 1984. *Assessment of confidence intervals for results of seismic hazard analysis*. In: Proc. 8th World Conf. Earthquake Engineering, vol. 1. San Francisco, pp. 263–270.
- Lagomarsino, S., Giovinazzi, S., 2006. Macroscopic and mechanical models for the vulnerability and damage assessment of current buildings. *Bull. Earthquake Eng.* 4, 415–443, <http://dx.doi.org/10.1007/s10518-006-9024-z>.
- Langenbruch, C., Shapiro, S., 2010. Decay rate of fluid-induced seismicity after termination of reservoir stimulations. *Geophysics* 75, MA53–MA62, <http://dx.doi.org/10.1190/1.3506005>.
- Majer, E.L., Baria, R., Stark, M., Oates, S., Bommer, J., Smith, B., Asanuma, H., 2007. Induced seismicity associated with enhanced geothermal systems. *Geothermics* 36, 185–222, <http://dx.doi.org/10.1016/j.geothermics.2007.03.003>.
- McGuire, R.K., 2008. Probabilistic seismic hazard analysis: early history. *Earthquake Eng. Struct. Dyn.* 37, 329–338, <http://dx.doi.org/10.1002/eqe.765>.
- Mena, B., Wiemer, S., Bachmann, C., 2013. Building robust models to forecast the induced seismicity related to geothermal reservoir enhancement. *Bull. Seismol. Soc. Am.* 103, 383–393, <http://dx.doi.org/10.1785/0120120102>.
- Mouroux, P., Le Brun, B., 2006. Presentation of RISK.UE Project. *Bull. Earthquake Eng.* 4, 323–339, <http://dx.doi.org/10.1007/s10518-006-9020-3>.
- Mukuhira, Y., Asanuma, H., Niitsuma, H., Häring, M.O., 2013. *Characteristics of large-magnitude microseismic events recorded during and after stimulation of a geothermal reservoir at Basel, Switzerland*. *Geothermics* 45, 1–17.
- Musson, R.M.W., Grünthal, G., Stucchi, M., 2010. The comparison of macroseismic intensity scales. *J. Seismol.* 14, 413–428, <http://dx.doi.org/10.1007/s10950-009-9172-0>.
- National Research Council, 2012. *Induced seismicity potential in energy technologies*. Available at: http://www.nap.edu/catalog.php?record_id=13355
- Ogata, Y., 1988. *Statistical models for earthquake occurrences and residual analysis for point processes*. *J. Am. Stat. Assoc.* 83, 9–27.
- Porter, K.A., Beck, J.L., Shaikhutdinov, R.V., 2002. Sensitivity of building loss estimates to major uncertain variables. *Earthquake Spectra* 18, 719–743.
- Ripperger, J., Kästli, P., Fäh, D., Giardini, D., 2009. Ground motion and macroseismic intensities of a seismic event related to geothermal reservoir stimulation below the city of Basel – observations and modelling. *Geophys. J. Int.* 179, 1757–1771, <http://dx.doi.org/10.1111/j.1365-246X.2009.04374.x>.
- Shapiro, S.A., Dinske, C., Kummerow, J., 2007. Probability of a given-magnitude earthquake induced by a fluid injection. *Geophys. Res. Lett.* 34, L22314, <http://dx.doi.org/10.1029/2007GL031615>.
- Shapiro, S.A., Dinske, C., 2009. Scaling of seismicity induced by nonlinear fluid-rock interaction. *J. Geophys. Res.* 114, B09307, <http://dx.doi.org/10.1029/2008JB006145>.
- Shapiro, S., Dinske, C., Langenbruch, C., Wenzel, F., 2010. Seismogenic index and magnitude probability of earthquakes induced during reservoir fluid stimulations. *Leading Edge* 29, 304–309, <http://dx.doi.org/10.1190/1.3353727>.
- Smith, M.C., 1983. *A history of hot dry rock geothermal energy systems*. *J. Volcanol. Geothermal Res.* 15, 1–20.
- Stirling, M., Litchfield, N., Gerstenberger, M., Clark, D., Bradley, B., Beavan, J., McVerry, G., Van Dissen, R., Nicol, A., Wallace, L., Buxton, R., 2012. Preliminary probabilistic seismic hazard analysis of the CO2CRC Otway Project Site, Victoria, Australia. *Bull. Seismol. Soc. Am.* 101, 2726–2736, <http://dx.doi.org/10.1785/0120110049>.
- swisstopo, 2012. *Federal Office of Topography, Swiss Confederation, Wabern b. Bern*.
- Ustaszewski, K., Schmid, S.M., 2007. Latest Pliocene to recent thick-skinned tectonics at the Upper Rhine Graben–Jura Mountains junction. *Swiss J. Geosci.* 100, 293–312, <http://dx.doi.org/10.1007/s00015-007-1226-0>.
- Walker, O., Dietz, S., 2012. *Ambiguity and insurance: robust capital requirements and premiums*. In: Grantham Research Institute on Climate Change and the Environment, Working Paper No. 97.
- Wiemer, S., 2001. *Introducing probabilistic aftershock hazard mapping*. *Geophys. Res. Lett.* 27, 3405–3408.
- Wiemer, S., Giardini, D., Fäh, D., Deichmann, N., Sellami, S., 2009. Probabilistic seismic hazard assessment of Switzerland: best estimates and uncertainties. *J. Seismol.* 13, 449–478, <http://dx.doi.org/10.1007/s10950-008-9138-7>.
- Woodward, R.T., Bishop, R.C., 1997. *How to decide when experts disagree: uncertainty-based choice rules in environmental policy*. *Land Econ.* 73, 492–507.
- Zoback, M., Gorelick, S.S., 2012. Earthquake triggering and large-scale geologic storage of carbon dioxide. *PNAS* 109, 10164–10168, <http://dx.doi.org/10.1073/pnas.1202473109>.